# Dopamine D$_2$, D$_3$, and D$_4$ Selective Phenylpiperazines as Molecular Probes To Explore the Origins of Subtype Specific Receptor Binding

Katharina Ehrlich,[†] Angela Gotz,[†,‡] Stefan Bollinger,[†] Nuska Tschammer,[†] Laura Bettinetti,[†] Steffen Harterich,[†] Harald Hubner,[†] Harald Lanig,[‡] and Peter Gmeiner*,[†]

[†]*Department of Chemistry and Pharmacy, Emil Fischer Center, Friedrich Alexander University, Schuhstrasse 19, 91052 Erlangen, Germany, and* [‡]*Department of Chemistry and Pharmacy, Computer Chemistry Center, Friedrich-Alexander-Universitat, Nagelsbachstrasse, 25, 91052 Erlangen, Germany*

Assembling phenylpiperazines with 7a-azaindole via different spacer elements, we developed subtype selective dopamine receptor ligands of types **1a,c**, **2a**, and **3a** preferentially interacting with D$_4$, D$_2$, and D$_3$, respectively. To complete this set, the methylthio analogues **2b** and **3b** exceeding the affinity of **2a** and **3a** by one order of magnitude and the structural intermediate **1b** were synthesized. These chemically similar but biologically divergent target compounds served as molecular probes for radioligand displacement experiments, mutagenesis, and docking studies on homology models based on the recent crystal structure of the $\beta_2$-adrenergic receptor. Specific interactions with the highly conserved amino acids Asp$^{3.32}$ and His$^{6.55}$ and less conserved residues at positions 2.61, 2.64, 3.28, and 3.29 were identified. Inclusion of a carefully modeled extracellular loop 2 displayed two nonconserved residues in EL2 that differently contribute to ligand binding. Obviously, subtype selectivity is caused by nonconserved but frequently mediated by conserved amino acids.

## Introduction

The D$_2$-like dopamine receptors including the subtypes D$_2$, D$_3$, and D$_4$ are members of the large family of G-protein-coupled receptors (GPCRs[a]), also referred to as seven transmembrane receptors. Many central nervous system diseases like schizophrenia, Parkinson's disease, drug addiction, and erectile dysfunction are associated with D$_2$-like dopamine receptors.[1]

Highly selective ligands are needed to specifically target receptor subtypes involved in these diseases. For example, D$_3$-selective drug candidates are discovered for the treatment of schizophrenia and drug addiction.[1-4] On the other hand, D$_4$-selective agonists and partial agonists facilitate a promising approach in the therapy of erectile dysfunction.[5-7] Therefore, knowledge about selectivity generating properties of the ligands and their receptors is important for drug design.

On the basis of rhodopsin, comparative molecular modeling of the D$_2$-like dopamine receptors and ligand docking revealed differences in the size and shape of a common ligand binding site when we and others suggested that particular microdomains in transmembrane helix 2 (TM2), TM3, and TM7 might be relevant for ligand selectivity.[1,8] These results are in accordance with mutagenesis studies, which also proposed changes in the hydrophobic interface between TM2, TM3, and TM7 to be liable for subtype selectivity at the D$_2$-like dopamine receptors.[9-11]

By application of CoMFA (comparative molecular field analysis) and CoMSIA (comparative molecular similarities indices analysis), 3D-QSAR studies guided us to a rational development of D$_3$-selective phenylpiperazines as radioligands for PET (positron emission tomography).[12-19]

Among aminergic GPCR ligands, phenylpiperazines are known as privileged structural moieties simulating native biogenic amines, like dopamine, serotonin, and (nor)epinephrine (Chart 1).[20] Containing an aromatic ring system and a basic nitrogen, the phenylpiperazine scaffold can be regarded as the primary recognition element targeting the neurotransmitter binding site of aminergic GPCRs.[21-24] Carbocyclic or heterocyclic appendages have been linked via a spacer element to enhance both affinity and subtype selectivity. We identified the 7a-azaindole system as an excellent heterocyclic moiety for D$_2$, D$_3$, and D$_4$ selective phenylpiperazines when subtype specificity could be controlled by the nature of the spacer element. Thus, use of an *N*-butylcarboxamide chain linking postion 2 of the azaindole ring with the phenylpiperazine moiety led to the D$_3$-selective partial agonist **3a** ($K_i$ = 4.3 nM, D$_3$/D$_2$ = 72, D$_3$/D$_4$ = 30). Interestingly, our SAR studies displayed that shortening of the spacer by one carbon and change of the substitution at the azaindole ring resulted in preferential D$_2$ binding when compared to D$_3$. Thus, the *N*-propylcarboxamide derivative **2a** revealed a $K_i$ of 11 nM compared to 150 nM of D$_3$ and 14 nM for D$_4$. On the other hand, we discovered highly selective D$_4$ receptor partial agonists and antagonists of type **1a** (FAUC 213, $K_i$ = 2.2 nM, D$_4$/D$_2$ = 1500; D$_4$/D$_3$ = 2400), **1c** and **1d** (FAUC 113) when using a methylene unit to link the primary recognition element

*To whom correspondence should be addressed. Phone: +49 9131 85-29383. Fax: +49 9131 85-22585. E-mail: peter.gmeiner@medchem.uni-erlangen.de.
[a] Abbreviations: GPCR, G-protein-coupled receptor; EL, extracellular loop; TM, transmembrane helix; CHO, Chinese hamster ovary; HEK, human embryonic kidney; HR-EIMS, high resolution electron ionization mass spectrometry; EI-MS, electron ionization mass spectrometry.
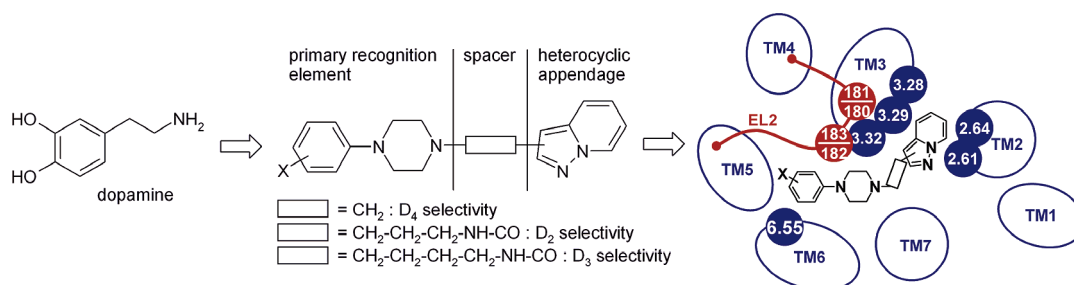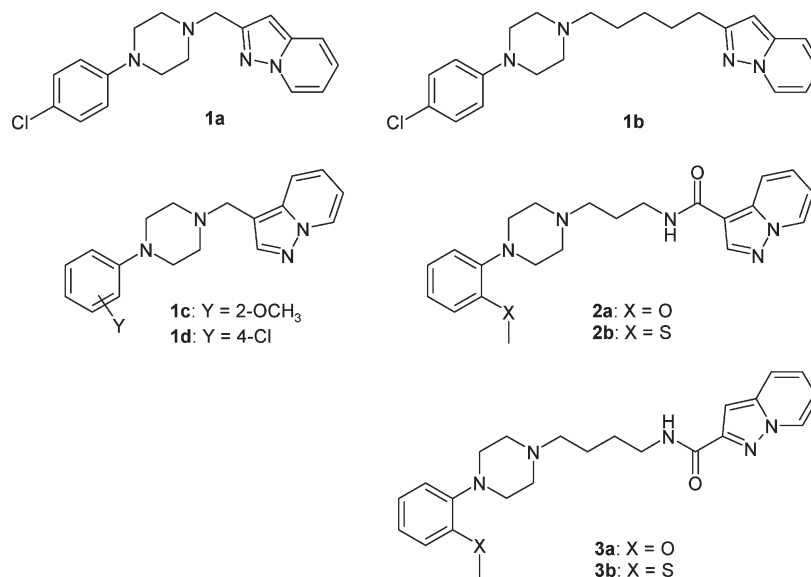
**Chart 1**



**Chart 2**



with the heterocyclic appendage (Chart 2).[5,25-28] Taking advantage of the finding that these target compounds show both high chemical similarity and significantly different biological binding patterns, we chose them as molecular probes to better understand the molecular origins of subtype selectivity. The identification of conserved and nonconserved residues that determine subtype selectivity of the binding pocket was based on previous SAR, mutagenesis, and docking studies. Whereas the phenylpiperazine substructure obviously simulates the biogenic amine, the data clearly indicate that the relative topicity of the heterocyclic appendage is responsible for subtype specific recognition.

Recent mutagenesis and preliminary docking studies suggest that two adjacent amino acid side chains in TM3 (3.28 and 3.29), two critical residues in TM2 (2.61 and 2.64), and two positions within EL2 are in proximity to the spacer elements and the heterocyclic appendages and, thus, determine subtype selectivity. For the primary recognition element, our preliminary molecular modeling results identified His$^{6.55}$ as a key residue for the interaction with the common phenylpiperazine unit. Finally, Asp$^{3.32}$ should be modified because its carboxylate function has been proved to be responsible for a reinforced H-bond provided by the basic nitrogen of the ligands.

Extending the above-mentioned dopamine receptor ligands by three further molecular probes to be synthesized, we herein describe mutagenesis studies and homology modeling of D$_2$, D$_3$, and D$_4$ based on the recent crystal structure of the β$_2$-adrenergic receptor.[29]

## Results and Discussion

**Compound Selection.** To be able to confirm that mutagesesis experiments are, in fact, diagnostic for a family of compounds, at least two representatives for each subtype should be investigated. Taking advantage of our in-house compound library, we identified an ortho-positioned methylthio group to be advantageous for dopamine receptor affinity. Because high binding affinity was expected to be beneficial for mutagenesis experiments, the test compounds **2b** and **3b** should be synthesized as structural analogues of methoxyphenylpiperazines **2a** and **3a**. As a structural intermediate between the methylene linked probe **1a** and the D$_2$ and D$_3$ selective *N*-alkylcarboxamides **2a** and **3a** (FAUC 329), respectively,[26] the pentylene bridged azaindole **1b** should be prepared. In analogy to the D$_2$ selective congeners **2a,b**, compound **1b** displays a five-atom spacer. However, a carboxamide function is replaced by an ethylene unit.

**Synthesis.** The azaindole derivative **2b** was synthesized as shown in Scheme 1. Nucleophilic substitution of 3-bromopropionitrile with 1-(2-methylsulfanylphenyl)piperazine (**4**) resulted in formation of the tertiary amine **5**. Reduction of the nitrile function with lithium aluminum hydride followed by TBTU mediated coupling of the resulting aminopropylpiperazine **6** with pyrazolo[1,5-*a*]pyridine-3-carboxylic acid gave the target compound **2b** (Scheme 1).[30,31]

To approach to the azaindole derivative **1b**, the building block **7** was reacted with 1-aminopyridinium iodide to give the heteroarene **8**.[32-35] Intermediate **8** was subjected to

hydrolysis and decarboxylation with 40% $H_2SO_4$ to afford **9**. Subsequent HOAt mediated DCC coupling with 1-(4-chlorophenyl)piperazine furnished the carboxamide **10**, which was reduced by $LiAlH_4$ to get the final product **1b** (Scheme 2). Test compounds **1a**, **1c**, **2a**, and **3a** were prepared according to our previously described protocols.[5,25,26,36]

**Ligand Binding.** Radioligand displacement assays were performed to determine binding affinities and the selectivity profiles of the new dopamine receptor ligands **1b**, **2b**, and **3b** in comparison to the described phenylpiperazines **1a,c**, **2a**, and **3a**. The binding data were generated by measuring the ligands' ability to compete with [³H]spiperone for the cloned

**Scheme 1**[a]
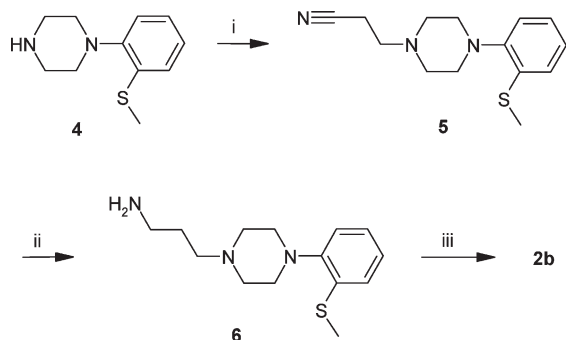


[a] Reaction conditions: (i) 3-bromopropionitrile, $K_2CO_3$, NaI, MeCN, reflux 24 h (67%); (ii) $Et_2O$, $LiAlH_4$, 0 °C to room temp, 1 h (18%); (iii) pyrazolo[1,5-*a*]pyridine-3-carboxylic acid, $CH_2Cl_2$, DIPEA, TBTU, 0 °C to room temp, 2 h (87%).

**Scheme 2**[a]
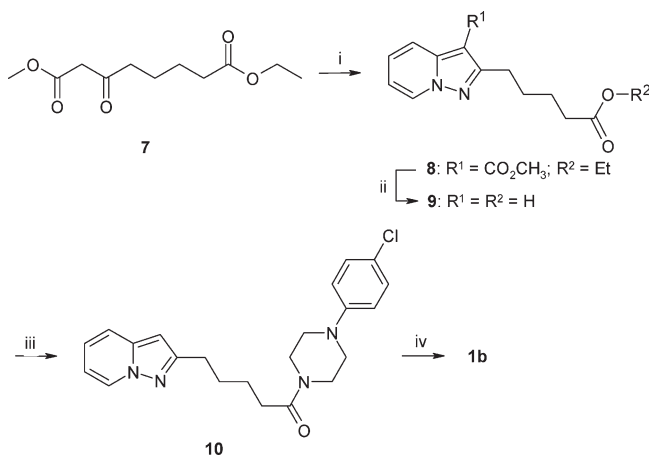


[a] Reaction conditions: (i) 1-aminopyridinium iodide, $K_2CO_3$, DMF, 50 °C, 2 h (13%); (ii) 40% $H_2SO_4$, 110 °C 3 h (93%); (iii) 1-(4-chlorophenyl)piperazine, DCC, HOAt, room temp, 15 h (81%); (iv) $LiAlH_4$, $Et_2O$, 0 °C, 1 h, to room temp, 5 h (59%).

human dopamine receptor subtypes stably expressed in CHO (Chinese hamster ovary) cells (Table 1). Formal exchange of the methoxy group of the preferential $D_2$ agonist **2a** by a methylthio group to give the methylthiophenylpiperazine **2b** resulted in an 8-fold increase in binding affinity and substantially improved selectivity over the $D_4$ subtype. An analogous exchange for the $D_3$ ligand **3a**, giving the thio analogue **3b**, resulted in a 12-fold increase in binding affinity at $D_3$. Elongation of the spacer of the small, highly $D_4$ selective ligand **1a** gave the structural intermediate **1b** which displayed a large decrease in affinity for the D4 receptor, whereas affinity for the $D_2$ and the $D_3$ receptor was increased when compared to **1a**.

**Modeling of the Dopamine $D_2$, $D_3$, and $D_4$ Receptors.** Receptor models of the dopamine $D_2$, $D_3$, and $D_4$ receptor were constructed using the crystal structure of the human $\beta_2$-adrenergic receptor (PDB entry 2RH1) as a template.[37] The artificially engineered intracellular loop 3 present in the crystal structure was omitted in receptor modeling, since it was found to have no direct effect on ligand binding.[38]

On the basis of agreement with experimental data, one receptor model was selected for each of the $D_2$ and the $D_3$ receptor, whereas for the $D_4$ receptor, two diverse models existed that showed different $\chi_1$ rotamers at Phe[2.61]. These two diverse models were chosen by docking experiments with the $D_4$-selective ligand **1a** and its 3-substituted regioisomer **1d**.[28]

In rhodopsin and in the $\beta_2$-adrenergic receptor, the part of the EL2 that is C-terminal to the conserved disulfide bond connecting EL2 and TM3 is involved in receptor−ligand interaction.[37,39] SCAM (substituted cysteine accessibility method) studies at the $D_2$ receptor also identified Ile184 to be involved in ligand binding.[40] Therefore, we decided to complete our $D_2$, $D_3$, and $D_4$ receptor structures by the inclusion of a carefully modeled EL2. The C-terminal region of the EL2, which is supposed to take part in ligand binding, was modeled according to the $\beta_2$-adrenergic crystal structure. The N-terminal region was selected from the loop database of the Swiss-PdbViewer.[41] The resulting structure was equilibrated by means of molecular dynamics simulation and energy minimization at a $D_4$ ligand−receptor complex. This loop was then reinserted into the original $D_4$ receptor model and also provided the basis for modeling of the EL2 at the $D_2$ and the $D_3$ receptor models. This procedure resulted in conformations of the EL2 that agreed with experimental data; the C-terminal end of EL2 is close to the binding site crevice; Ile184 in $D_2$, Ile183 in $D_3$, and Leu187 in $D_4$ point into the binding pocket, thereby enabling interactions with the ligand.

**Ligand Docking and Analysis.** The final receptor models were used for docking experiments by means of AUTO-DOCK4. The high affinity ligands **2b**, **3a**, and **1a** were docked in the $D_2$, $D_3$, and $D_4$ receptor model, respectively.

**Table 1.** Receptor Binding and Selectivity Ratios for **1a**−**3b**

| | | | $K_i$[a][³H]spiperone | | | ratio of $K_i$ values | | |
|---|---|---|---|---|---|---|---|---|
| compd | X | position | $D_{2L}$ | $D_3$ | $D_4$ | $D_{2L}/D_3$ | $D_2/D_4$ | $D_3/D_4$ |
| **1a**[b] | | 2 | 3400 ± 450 | 5300 ± 720 | 2.2 ± 0.23 | 0.64 | 1500 | 2400 |
| **1b** | | 2 | 160 ± 90 | 370 ± 40 | 46 ± 5.2 | 0.43 | 3.5 | 8.0 |
| **1c**[c] | | 3 | 280 ± 130 | 1200 ± 240 | 1.2 ± 0.2 | 0.23 | 230 | 1000 |
| **2a**[d] | O | 3 | 11 ± 1.4 | 150 ± 17 | 14 ± 2.5 | 0.07 | 0.79 | 11 |
| **2b** | S | 3 | 1.4 ± 0.26 | 18 ± 2.5 | 8.8 ± 1.4 | 0.08 | 0.16 | 2.0 |
| **3a**[d] | O | 2 | 310 ± 34 | 4.3 ± 0.29 | 130 ± 16 | 72 | 2.4 | 0.033 |
| **3b** | S | 2 | 16 ± 2.2 | 0.35 ± 0.036 | 65 ± 11 | 46 | 0.25 | 0.005 |

[a] $K_i$ ± SEM, in nM, are based on the mean values of 2−9 experiments each done in triplicate. [b] Reference 25. [c] Reference 5. [d] Reference 26.
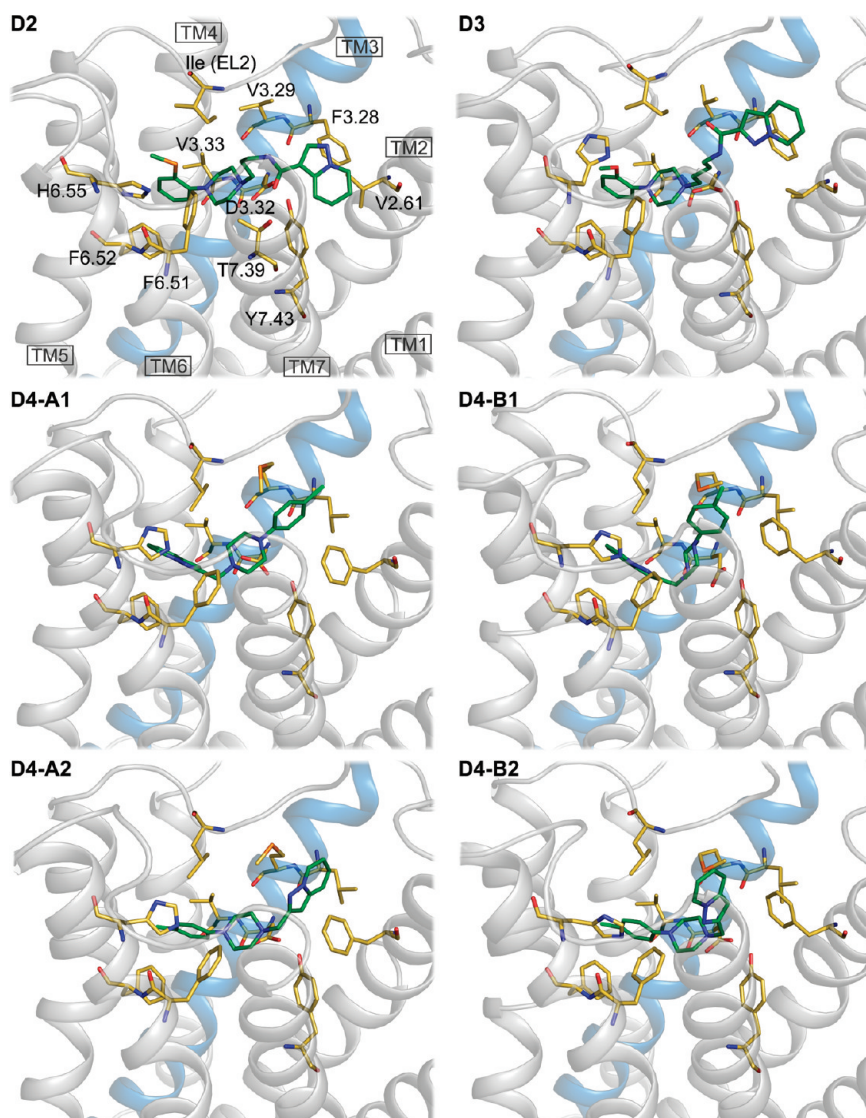
**Figure 1.** Phenylpiperazines of types **1a**, **2b**, and **3a** docked into the respective $D_2$, $D_3$, and $D_4$ receptor models. Residues involved in ligand binding and the ligands are represented as sticks. Receptor backbone is represented as gray ribbon, except for TM3 which is colored blue, for clarity. $D_2$ and $D_3$ ligand−receptor complexes as well as four different $D_4$ ligand−receptor complexes (two receptor models with two binding modes, each) are displayed.

Only ligand−receptor complexes in which the protonated nitrogen of the phenylpiperazine scaffold established an essential charge reinforced H-bond with $Asp^{3.32}$ were considered. The resulting receptor−ligand complexes were clustered and scored by Drugscore[online].[42] After a final selection according to experimental data, the best receptor−ligand complexes were subjected to energy minimization. The minimized complexes are shown in Figure 1.

In addition to the polar interaction with $Asp^{3.32}$, all ligands interacted with two receptor microdomains. The first microdomain comprises the less conserved residue $His^{6.55}$ in TM6 and the highly conserved residues $Trp^{6.48}$, $Phe^{6.51}$, $Phe^{6.52}$, and $Val^{3.33}$ in TM6 and TM3, respectively. The second microdomain consists of residues in TM7 ($Thr^{7.39}$, $Trp^{7.40}$, and $Tyr^{7.43}$) and at positions 2.61, 2.64, 3.28, and 3.29 at TM2 and TM3, respectively.

Docking of the preferential $D_2$ ligand **2b** into the $D_2$ receptor model yielded a receptor−ligand complex in which the methylthiophenyl moiety of **2b** lies in a lipophilic pocket formed by TM3, TM5, TM6 and capped by EL2. The methylthio group

is in proximity to $His^{6.55}$ and Ile184 originating from EL2. The amide group interacts with $Thr^{7.39}$ via the carbonyl oxygen. The azaindole moiety points toward TM2 and interacts with a lipophilic microdomain formed by Ile183 from EL2, $Val^{2.61}$, $Leu^{2.64}$, and $Trp^{7.40}$.

The $D_3$ selective ligand **3a** was docked into the $D_3$ receptor model. Analogous to the orientation of **2b** in the $D_2$ receptor model, the methoxyphenyl moiety of **3a** interacts with critical residues in TM5, TM6, Ile183 in EL2, and $Val^{3.33}$ in TM3. It is worthy of note that the methoxy group was positioned in proximity to $His^{6.55}$. The heterocyclic moiety points toward TM2, interacting with a hydrophobic cluster formed by Val180 from EL2, and $Leu^{2.64}$.

Ligands of types **2** and **3** interact in a very similar binding mode with the $D_2$ and $D_3$ binding site, respectively, with the phenylpiperazine moiety pointing toward TM5 and the methoxy or methylthio substituent pointing toward an isoleucine originating from the EL2 (Figure 2). The heterocyclic arene moiety, however, interacts differently at the $D_2$ and the $D_3$ ligand−receptor complexes. The azaindole
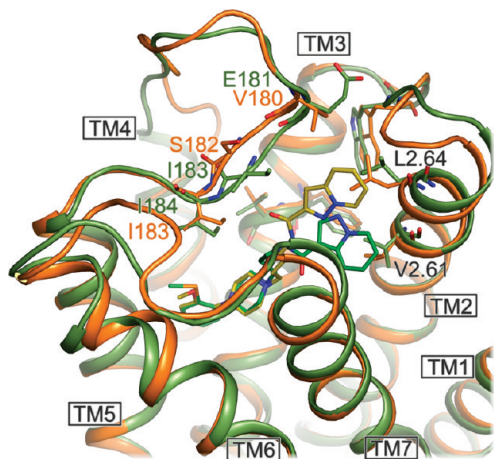
**Figure 2.** Ligand binding at the EL2. Representation of the $D_2$ (green) and the $D_3$ (orange) ligand— receptor complexes. Hydrophobic residues from EL2 and the hydrophobic cluster at TM2 and TM3 (Val$^{2.61}$, Leu$^{2.64}$, Trp100/Trp96 from EL1, Phe$^{3.28}$, Val$^{3.29}$) are shown as sticks. Important residues and sequence differences at the EL2 are highlighted by residue numbers.

of the preferential $D_2$ ligand **2b** interacts with Val$^{2.61}$, Leu$^{2.64}$, Trp$^{7.40}$, and Ile183 from the EL2. The elongated heterocyclic appendage of the $D_3$ selective ligand **3a** stretches further toward the extracellular side, interacting primarily with Leu$^{2.64}$, and Val180 from the EL2. The position of Ile183 at the $D_2$ receptor is occupied by Ser182 at the $D_3$ receptor, whereas Val180 of the $D_3$ receptor corresponds to Glu181 at the $D_2$ receptor (Figure 2). Both residues are located next to the conserved cysteine, forming a disulfide bond with Cys$^{3.25}$ from TM3. These differences within the ligand binding pocket are specifically addressed by the heterocyclic appendage of the respective $D_2$ and $D_3$ selective receptor ligands. We therefore presume that these nonconserved residues are directly involved in $D_2/D_3$ subtype selectivity and that the heterocyclic appendage greatly contributes to subtype selectivity.

The $D_4$ selective phenylpiperazine **1a** was docked into two relevant $D_4$ receptor models (A and B). In model A, Phe$^{2.61}$ is oriented toward TM7, thereby facilitating interactions between the ligand and residues originating from TM3. In model B, Phe$^{2.61}$ points toward TM3 partly obstructing interactions between the ligand and TM3. Docking resulted in two alternative orientations of **1a** in both models A and B. In mode-1, the azaindole moiety interacts with the lipophilic pocket formed by aromatic residues in TM6, Leu187 in EL2, and Val$^{3.33}$ in TM3. The chlorophenyl moiety, however, interacts differently in both models. In model A, the aromatic moiety is situated between Phe$^{2.61}$ and TM3 interacting with the hydrophobic microdomain formed by Phe$^{2.61}$, Leu$^{3.28}$, and Met$^{3.29}$, whereas in model B the conformation of Phe$^{2.61}$ hinders the interaction between the ligand and Leu$^{3.28}$.

Mode-2 is similar to the orientation of the long chain analogues **2b** and **3a** in the $D_2$ and $D_3$ receptor model, respectively. The chlorophenyl moiety interacts with the hydrophobic microdomain that spans the TM6 and TM3 interface, and the chloro substituent points at TM5. In model A, the azaindole moiety lies between Phe$^{2.61}$ and TM3, interacting with the hydrophobic cluster at the TM2—TM3 interface. In model B, the heteroarene points at TM7 lacking the interaction with Val$^{3.29}$. In a comparison of mode-1 and mode-2, the position of the charged nitrogen of **1a** varies by $2-3$ Å.

In summary, docking of the phenylpiperazines **2b** and **3a** into our $D_2$ and $D_3$ models, respectively, yielded one ligand—receptor complex each. The substituted phenyl moiety displays favorable interactions with a lipophilic cluster in TM6, whereas the azaindole moiety points at TM2. Docking of the methylene-bridged test compound **1a** into $D_4$ resulted in two alternative orientations. In mode-1, the heteroarene moiety interacts with the aromatic residues in TM6 and the chlorophenyl moiety is involved in interactions with TM2 and TM3. In mode-2, the chlorophenyl moiety lies within the hydrophobic pocket formed by TM6 and TM3 whereas the pyrazolopyridine moiety interacts with a hydrophobic cluster at the TM2—TM3 interface. Although scoring values of $D_4$-A2, showing an orientation of the ligand analogous to the $D_2$ and $D_3$ ligand—receptor complexes, were much better than those of $D_4$-A1, previous experimental data could not yet prove in which orientation type **1** ligands bind to the dopamine $D_4$ receptor. Because of the symmetry of the short methylene-bridged ligand, both binding modes are conceivable. Experiments published by Schetz et al. revealed earlier that small changes at the ligand can cause a switch from mode-1 in which the azaindole moiety is oriented toward TM5 (models $D_4$-A1 and $D_4$-B1) to mode-2 in which the phenylpiperazine points toward TM5 (models $D_4$-A2 and $D_4$-B2).[10] According to our studies, the observed heterogeneity in the binding mode and the 4-chloro substitution of the phenylpiperazine moiety led to a deviation in the position of the basic amine and its interaction with Asp$^{3.32}$ compared to the $D_2$ and $D_3$ ligand—receptor complexes. We suggest that the binding mode of the elongated structural analogue **1b** resembles mode-2. Because of its longer spacer arm, the basic amine of the phenylpiperazine scaffold is no longer at the center of the molecule but further away from the azaindole. In mode-1, the longer distance would impede the simultaneous interaction with Asp$^{3.32}$ and the aromatic/hydrophobic pocket formed at TM3, TM5, and TM6.

**Receptor Mutagenesis.** Site directed mutagenesis was applied in the $D_2$ and $D_3$ dopamine receptor background to determine the influence of selected residues on ligand binding and subtype selectivity. Thus, diagnostic amino acids of $D_2$ and $D_3$ were mutated and mutant receptors transiently expressed in HEK 293 cells. To characterize the binding properties, saturation experiments were conducted to determine $B_{max}$ and $K_D$ values. Subsequently, the impact on the recognition properties of our test compounds **1a**−**c**, **2a,b**, and **3a,b** was investigated when comparing binding affinities with those of transiently expressed wildtype receptor protein. The binding site crevice of $D_2$-like receptors is expected to be lined by several highly conserved amino acids, among which Asp$^{3.32}$, Ser$^{5.42}$, Ser$^{5.43}$, Ser$^{5.46}$, Phe$^{6.51}$, Phe$^{6.52}$, and Tyr$^{7.43}$ seem to be of crucial importance.[1,43−46] These results are now corroborated by the recent GPCR crystal structures.[29,47,48] However, nonconserved residues within or next to the binding pocket have the highest probability to be involved in subtype selectivity. On the basis of our computational predictions, we selected four residues, differentiating the $D_2$ and $D_3$ from the $D_4$ receptor (positions 2.61, 2.64, 3.28, and 3.29), and two residues from EL2, differentiating the $D_2$ from the $D_3$ subtype (Glu181/Val180 and Ile183/Ser182). But we also examined the key contacts of the conserved amino acids Asp$^{3.32}$ and His$^{6.55}$ that were expected to interact with the cationic ammonium center and the catechol bioisostere, respectively. Asp$^{3.32}$ is regarded to be essential for ligand binding at aminergic GPCRs but might differ in its contribution to ligand binding

**Table 2.** $K_d$ and $B_{max}$ Values at Wild Type and Mutant Receptors[a]

| | $D_{2L}$ receptor | | $D_3$ receptor | |
| --- | --- | --- | --- | --- |
| mutation | $K_d$[b] | $B_{max}$[c] | $K_d$[b] | $B_{max}$[c] |
| wild type | 0.44 ± 0.06 | 1600 ± 180 | 0.54 ± 0.07 | 1600 ± 180 |
| D3.32E | 0.34 ± 0.09 | 1300 ± 230 | 2.0 ± 0.20 | 390 ± 89 |
| V2.61F | 0.75 ± 0.16 | 1100 ± 200 | 0.55 ± 0.08 | 1600 ± 200 |
| L2.64F | 0.53 ± 0.15 | 2500 ± 760 | 0.54 ± 0.12 | 330 ± 53 |
| FV3.28,3.29LM | 1.3 ± 0.24 | 2200 ± 440 | 0.81 ± 0.17 | 12009 ± 160 |
| V2.61F+FV3.28,3.29LM | 0.67 ± 0.19 | 2300 ± 360 | 0.84 ± 0.09 | 2200 ± 270 |
| $D_2$E181 V+I183S | 1.1 ± 0.24 | 1900 ± 340 | | |
| $D_3$V180E+S182I | | | 0,70 ± 0.04 | 290 ± 100 |
| H6.55A | 0.41 ± 0.09 | 1600 ± 310 | 1.0 ± 0.13 | 1200 ± 170 |
| H6.55F | 0.86 ± 0.13 | 1400 ± 500 | NBD[d] | NBD[d] |

[a] Values were determined by saturation binding experiments with [³H]spiperone at receptors transiently expressed in HEK 293 cells. [b] $K_d$ ± SEM values, in nM, are based on the mean of 2−43 independent experiments each done in triplicate. [c] $B_{max}$ in fmol/mg protein. [d] NBD = no binding detected.

**Table 3.** Binding Data of Compounds **1a−c**, **2a,b**, and **3a,b** at Wild Type and Mutant Receptors ($K_i$ values ± SEM in nM)[a]

| receptor | 1a | 1b | 1c | 2a | 2b | 3a | 3b |
| --- | --- | --- | --- | --- | --- | --- | --- |
| $D_2$wt | 2300 ± 360 | 220 ± 46 | 350 ± 83 | 13 ± 2.8 | 2.2 ± 0.4 | 150 ± 35 | 37 ± 7 |
| $D_2$D3.32E | 5100 ± 360 (2.2) | | 1500 ± 130 (4.4) | 720 ± 140 (55) | 160 ± 29 (74) | 3500 ± 240 (23) | 1300 ± 75 (34) |
| $D_2$V2.61F | 1200 ± 220 (0.53) | 740 ± 140 (3.3) | 94 ± 32 (0.27) | 450 ± 75 (34) | 100 ± 25 (45) | 920 ± 230 (6.0) | 130 ± 6.0 (3.4) |
| $D_2$L2.64F | 2000 ± 200 (0.89) | | 610 ± 100 (1.8) | 390 ± 70 (30) | 660 ± 92 (303) | 940 ± 38 (6) | 120 ± 17 (3) |
| $D_2$FV3.28,3.29LM | 300 ± 61 (0.13) | 1100 ± 250 (4.9) | 46 ± 3.5 (0.13) | 110 ± 11 (8.5) | 35 ± 7 (16) | 220 ± 53 (1.4) | 65 ± 15 (1.8) |
| $D_2$V2.61F+ FV3.28,3.29LM | 66 ± 14 (0.03) | 470 ± 90 (2.1) | 54 ± 8 (0.15) | 83 ± 26 (6) | 20 ± 8 (9) | 120 ± 7.5 (0.81) | 26 ± 1.0 (0.70) |
| $D_2$E181 V+I183S | 47000 ± 19000 (19) | | 3600 ± 460 (10.5) | 81 ± 6.6 (6.2) | 26 ± 3.8 (12) | 1000 ± 250 (6.8) | 130 ± 23 (3.4) |
| $D_2$H6.55A | 320 ± 100 (0.14) | 170 ± 29 (0.74) | 63 ± 5 (0.18) | 1.6 ± 0.40 (0.12) | 0.1 ± 0.014 (0.05) | 21 ± 1.1 (0.14) | 11 ± 0.6 (0.3) |
| $D_2$H6.55F | 1600 ± 550 (0.7) | | 590 ± 100 (1.2) | 69 ± 15 (5.3) | 17 ± 4 (7.7) | 340 ± 69 (2.2) | 160 ± 43 (4.3) |
| $D_3$wt | 8300 ± 1200 | 220 ± 52 | 770 ± 38 | 320 ± 61 | 26 ± 4 | 7.4 ± 1.1 | 0.5 ± 0.08 |
| $D_3$D3.32E | 12000 ± 1900 (1.4) | | 680 ± 100 (0.9) | 390 ± 61 (1.2) | 650 ± 67 (25) | 93 ± 9.0 (13) | 230 ± 21 (466) |
| $D_3$V2.61F | 9200 ± 1700 (1.1) | 1900 ± 460 (8.8) | 2300 ± 110 (3.0) | 1030 ± 170 (3.3) | 740 ± 100 (29) | 500 ± 81 (68) | 58 ± 12 (116) |
| $D_3$L2.64F | 1600 ± 170 (0.19) | | 720 ± 140 (0.9) | 630 ± 120 (2) | 430 ± 110 (17) | 290 ± 47 (40) | 33 ± 8.5 (66) |
| $D_3$FV3.28,3.29LM | 730 ± 85 (0.09) | 530 ± 120 (2.4) | 44 ± 3 (0.06) | 640 ± 140 (2.0) | 320 ± 34 (12) | 97 ± 4 (13) | 18 ± 3 (36) |
| $D_3$V2.61F+ FV3.28,3.29LM | 76 ± 10 (0.009) | 1100 ± 260 (5.1) | 51 ± 11 (0.07) | 34 ± 7 (0.11) | 8 ± 0.9 (0.31) | 130 ± 19 (18) | 40 ± 12 (80) |
| $D_3$V180E+S182I | 2500 ± 1100 (0.31) | | 340 ± 59 (0.44) | 16 ± 4 (0.05) | 3.4 ± 0.99 (0.13) | 7.6 ± 1.5 (1.0) | 0.76 ± 0.11 (1.5) |
| $D_3$H6.55A | 46 ± 3.3 (0.005) | | 61 ± 1.0 (0.08) | 56 ± 11 (0.18) | 12 ± 3 (0.5) | 2 ± 0.21 (0.27) | 0.63 ± 0.15 (1.3) |
| $D_4$wt | 6.8 ± 0.7 | 46 ± 5[b] | 2.3 ± 0.3 | 52 ± 8 | 26 ± 3.4 | 400 ± 38 | 310 ± 43 |

[a] Binding data of compounds **1a−c**, **2a,b**, and **3a,b** were determined in competition binding experiments with [³H]spiperone at wild type and mutant receptors transiently expressed in HEK 293 cells. Values given are mean $K_i$ values ± SEM, in nM, of 2−18 independent experiments each done in triplicate. Fold changes in affinity compared to those of wild type are indicated in parentheses. [b] Binding data determined in competition binding experiments with [³H]spiperone at wild type stably expressed in CHO cells.

at the different receptor subtypes.[49] His[6.55] is conserved among the $D_2$-like dopamine receptors and involved in binding of dopamine, whereas no effect on binding of butyrophenone ligands could be detected upon mutation to cysteine or leucine.[50−52]

Except for $D_2$D3.32N and $D_3$H6.55F, our mutations had no noteworthy effect on binding of [³H]spiperone, a ligand that does not show subtype selectivity. As apparent from the $B_{max}$ values, expression levels remained unchanged and showed only minor fluctuations. Altogether, binding of [³H]spiperone was hardly influenced at our $D_2$ and $D_3$ receptor mutants, thereby distinguishing itself as the ideal radioligand for competition binding studies (Table 2).

To probe specific receptor ligand interactions of the ligands' cationic ammonium center, the highly conserved Asp[3.32] was mutated to glutamate at $D_2$ and $D_3$ receptors ($D_2$D3.32E, $D_3$D3.32E), which was least likely to disturb the protein structure either locally or in its overall folding pathway according to the guidelines for "safe amino acid substitution".[43,53,54] In fact, the $B_{max}$ value of $D_2$D3.32E was comparable to that of wild type (Table 2). On the other hand, mutation of Asp[3.32] to asparagine resulted in a complete loss of [³H]spiperone binding at the $D_2$ receptor, thereby excluding further experiments with test compounds at this mutant

receptor. While elongation of the amino acid side chain by one $CH_2$ group was tolerated, the acid functionality itself seems to be essential for the binding of the radioligand.

Compared to the $D_2$ wild type receptor, the exchange of aspartate by glutamate resulted in a 55-fold and a 74-fold decrease in affinity for the preferential $D_2$ ligands **2a** and **2b**, respectively (Table 3). At the $D_3$ receptor, **2a** was unaffected by $D_3$D3.32E, while **2b** exhibited a 25-fold decrease in affinity. The $D_3$ selective phenylpiperazine **3a** displayed a 23-fold and 13-fold drop in affinity and its thio analogue **3b** a 34-fold and 466-fold drop in affinity at the respective $D_2$D3.32E and $D_3$D3.32E receptor mutants. The $D_4$ selective compounds **1a** and **1c** showed a significant change in binding affinity at neither the $D_2$D3.32E nor the $D_3$D3.32E receptor mutant.

Asp[3.32] is one of the most conserved amino acids among aminergic GPCRs and is supposed to form a reinforced hydrogen bond with the basic amine of the ligand.[49] Interestingly, the $D_4$ selective compounds **1a** and **1c** were not affected by the D3.32E mutations at the $D_2$ and $D_3$ receptors. Ligands showing a low $K_i$ value, however, seem to be more affected by the D3.32E mutant receptors. It may be assumed that selectivity involves tight binding at a specific receptor subtype. This strict binding mode is very susceptible to small

changes, whereas at subtypes bound with lower affinity the substitution of Asp$^{3.32}$ by glutamate is easily tolerated.

Since preliminary molecular modeling studies indicated spatial proximity to the arene part of the phenylpiperazine unit, we decided to change His$^{6.55}$ into alanine at the D$_2$ and the D$_3$ receptor, thereby eliminating both its aromatic and basic side chain properties (D$_2$H6.55A, D$_3$H6.55A). Interestingly, our test compounds exhibited a gain in affinity at both the D$_2$H6.55A and the D$_3$H6.55A receptor mutants. The most prominent result was a 180-fold increase in affinity for the phenylpiperazine **1a** at D$_3$H6.55A. The mutation into phenylalanine (H6.55F) led to a complete loss of radioligand binding at the D$_3$ receptor, thereby excluding further experiments with this mutant. H6.55F mutation in the D$_2$ receptor background led to a decrease in affinity for the D$_2$ selective ligands **2a,b**, whereas the affinity of **1a** and **3a,b** was hardly affected.

His$^{6.55}$ is positioned one helix turn above Phe$^{6.52}$ and Phe$^{6.51}$, two highly conserved residues taking part in ligand binding. We suppose that the additional space created by the H6.55A mutation leads to an increase in conformational freedom of these two phenylalanine residues, thereby enabling a better accommodation of the phenylpiperzine moiety to the aromatic microdomain of TM6. The observed loss of binding at the D$_2$H6.55F mutant receptor further supports this hypothesis as exchange of His$^{6.55}$ by a sterically more demanding phenylalanine leads to less conformational freedom of Phe$^{6.52}$ or Phe$^{6.51}$, thereby hindering favorable receptor−ligand interactions.

The described D$_2$ model clearly showed an aberration from the D$_3$ and D$_4$ receptor models at the helix turn containing His$^{6.55}$. Phe$^{7.38}$, which is represented by a threonine at the D$_3$ and D$_4$ subtypes, sterically interacts with Thr$^{6.54}$, resulting in a sideward shift of the helix turn containing Thr$^{6.54}$ and His$^{6.55}$. At the D$_2$ model, the latter points downward in the direction of the ligand binding site, whereas at the D$_3$ receptor model, His$^{6.55}$ stretches upward in the direction of the EL2. This upward position enables the sp$^2$ nitrogen of the imidazole ring to accept an H-bond from the side chain of Tyr$^{7.35}$ (Figure 3). Although the residues involved in ligand binding are conserved, nonconserved residues in EL2 and at the TM6/TM7 helical interface lead to a subtype specific difference in the spatial arrangement next to the binding site. This explains why the H6.55F mutation was tolerated at the D$_2$ receptor, while at the D$_3$ receptor, it led to a complete loss of radioligand binding.

A similar effect was also observed in the direct comparison of the $\beta_1$ and $\beta_2$ adrenergic receptor crystal structures. All residues involved in ligand binding are conserved, but differences at more distant receptor sites are supposed to provide subtype selectivity, be it by influencing the conserved residues' rotameric states, binding kinetics, or receptor dynamics.[29,47] Extensive molecular modeling studies of the D$_2$-like dopamine receptors also indicated a different behavior and differing proline kink angles within the transmembrane helices, influencing the geometrical properties of the ligand binding site.[1] Therefore, nonconserved residues though distant from the ligand binding site can have a substantial influence on selectivity by changes in local or even overall geometry.

To gain further insight into the determinants of D$_2$/D$_4$ and D$_3$/D$_4$ ligand selectivity and to probe the molecular interactions of the heterocyclic appendages including parts of the spacer element, we decided to change Val$^{2.61}$, Phe$^{3.28}$, and Val$^{3.29}$,
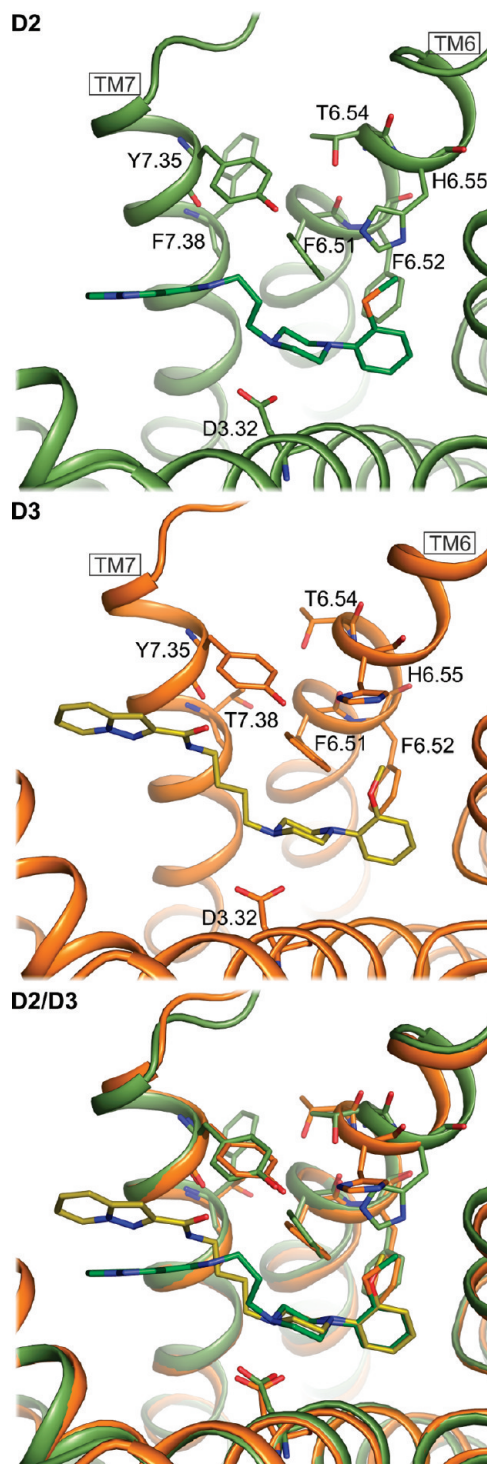


**Figure 3.** Differences between the D$_2$ and D$_3$ receptor models at His$^{6.55}$. Representation of the D$_2$ (green) and D$_3$ (orange) receptor models including the docked ligands. The EL2 was omitted for clarity. Important residues from TM6 and TM7 and Asp$^{3.32}$ are shown as sticks. The images display the influence of the interaction between positions 7.38 and 6.54 on the position and orientation of His$^{6.55}$.

which are conserved among the D$_2$ and D$_3$ receptors, into the corresponding amino acids present at the D$_4$ receptor.

Starting from both D$_2$ and D$_3$ wildtype, we constructed the mutants V2.61F and FV3.28,3.29LM and the triple mutant V2.61F+FV3.28,3.29LM, which were reported to be involved in D$_2$/D$_4$ subtype selectivity.[11]
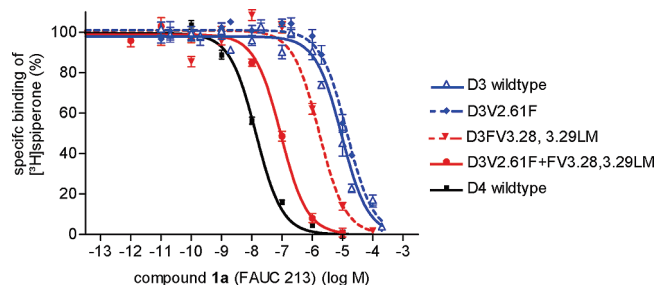
**Figure 4.** Radioligand displacement curves of **1a** at the $D_3$ and $D_4$ wild type and the $D_3V2.61F$, $D_3FV3.28,3.29LM$, and $D_3V2.61F+$FV3.28,3.29LM mutant receptors. Data shown are normalized results of competitive binding assays, showing the shift in affinity from $D_3$ toward $D_4$ receptor upon mutation at $Val^{2.61}$, $Phe^{3.28}$, and $Val^{3.29}$ of the $D_3$ receptor.
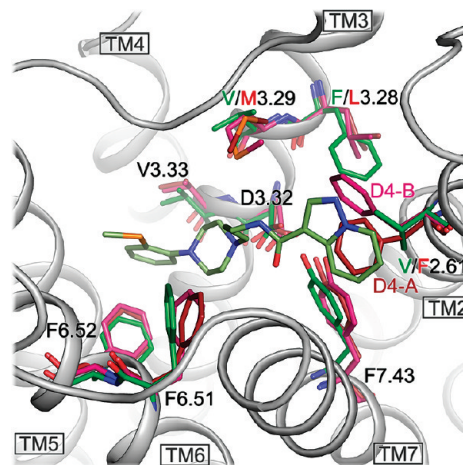


**Figure 5.** Receptor mutants at TM2 and TM3. Representation of the different spatial arrangement within the ligand binding site at positions 2.61, 3.28, and 3.29. The backbone of the $D_4$ receptor model A is shown as gray ribbon. Important residues (green, $D_2$; dark-red, $D_4$ model A; pink, $D_4$ model B) and compound **2b** docked into the $D_2$ receptor (olive green) are shown as sticks. This figure highlights the steric influence of the amino acid in position 3.28 on the conformation of $Phe^{2.61}$ and its interaction with the docked ligand.

In accordance with previously recorded mutagenesis data,[11] the single mutant V2.61F had hardly any effect on binding of **1a** and the double mutant FV3.28,3.29LM exhibited an 8-fold and 11-fold increase in affinity in the $D_2$ and $D_3$ background, respectively. Because of the $D_4$ like recognition properties, the affinity of the $D_4$ ligand **1a** was improved 35-fold and 109-fold at $D_2V2.61F+FV3.28,3.29LM$ and $D_3V2.61F+FV3.28,3.29LM$, respectively (Figure 4). The $D_4$ selective methoxyphenylpiperazine derivative **1c** also improved in affinity at the double and the triple mutants. On the other hand, the structural homologue **1b** incorporating an elongated spacer arm exhibited a 2- to 9-fold loss of binding affinity at the mutant receptors.

While the mutation V2.61F had no noteworthy effect on the phenylpiperazine **1a** and **1c**, the long chain analogues **2a,b** and **3a,b** displayed a substantial loss of binding affinity. The susceptibility of FV3.28,3.29LM on ligand binding of **2a,b** and **3a,b** was very similar but less pronounced. For both cases, the impact on ligands with high affinity was significantly higher than on poor binders.

As expected, a negative effect on ligand binding was observed for the preferential $D_2$ ligands **2a,b** at the $D_2V2.61F+FV3.28,3.29LM$ and the $D_3$ selective phenylpiperazines **3a,b** at the $D_3V2.61F+FV3.28,3.29LM$ receptor mutant. Because of the low affinity at the wild types, significant loss of binding could not be detected for **2a,b** in the $D_3$ and for **3a,b** in the $D_2$ background.

For a further validation of our binding hypothesis, $Leu^{2.64}$ was also mutated into the sterically more demanding amino acid phenylalanine. The mutation exhibited a distinct decrease in affinity for the preferential $D_2$ ligands **2a,b** at the $D_2L2.64F$ and the $D_3$ selective phenylpiperazines **3a,b** at the $D_3L2.64F$ receptor mutants. Affinity of the shorter $D_4$ ligands **1a,c** was hardly affected.

Our molecular docking experiments showed that the phenylpiperazine moiety of the longer $D_2$ and $D_3$ ligands binds to a primary recognition site provided by crucial microdomains of TMs 3, 5, and 6 forming the described favorable contacts with $Asp^{3.32}$, $Val^{3.33}$, $Trp^{6.48}$, $Phe^{6.51}$, $Phe^{6.52}$, and $His^{6.55}$. The heterocyclic arene moiety resides within a hydrophobic region at the TM2/TM3 interface which cannot be reached by the shorter $D_4$ selective compounds. This hydrophobic interface mainly consists of positions 3.28, 3.29, 2.64, 2.61 and a conserved tryptophane from the EL1. Mutation of $Leu^{2.64}$ or $Val^{2.61}$ to phenylalanine partly blocks this hydrophobic pocket which explains the observed loss of affinity. Conformational freedom of $Phe^{2.61}$

is restricted by steric interactions with $Phe^{3.28}$, which is still present at the $D_2$ and $D_3$ receptor mutant V2.61F. We suggest that the resulting conformation of $Phe^{2.61}$ is similar to the one observed in our $D_4$ receptor model A ($D_4$-A), which would lead to disadvantageous steric interactions with **2b** as docked into the $D_2$ receptor model (Figure 5). Additional mutation of $Phe^{3.28}$ and $Val^{3.29}$ to the sterically less demanding amino acids leucine and methionine, respectively, allows $Phe^{2.61}$ to move out of the ligand's way, adopting a conformation similar to the one observed in the $D_4$ receptor model B ($D_4$-B). This hypothesis is further supported by our experimental data indicating a negative effect of the mutation V2.61F on ligand binding compared to wild type but no effect or even an improvement in binding affinity when comparing FV3.28,3.29LM with V2.61F+FV3.28,3.29LM mutant receptors. Additionally, our $D_4$ receptor modeling indicates the propensity of $Phe^{2.61}$ to exist in two different rotameric states ($D_4$-A and $D_4$-B). Thus, binding affinity seems to be specifically generated by the heterocyclic appendage and the linker system and is substantially perturbed by the mutation at position 2.61.

The shorter $D_4$ ligands do not stretch that far into the hydrophobic pocket at TM2/TM3 but interact directly with $Phe^{2.61}$, $Leu^{3.28}$, and $Met^{3.29}$. Interestingly, the effect of the mutation at $Val^{2.61}$ on the binding affinity of $D_4$ selective compounds (**1a,c**) is similar when comparing wild type to V2.61F and FV3.28,3.29LM to V2.61F+FV3.28,3.29LM. This leads to the assumption that the aforementioned conformational changes at $Phe^{2.61}$, depending on the amino acid at position 3.28, do not occur for the binding of $D_4$ ligands, thus indicating model $D_4$-A. These conclusions are corroborated by the fact that the scoring values of model $D_4$-A were significantly better than those of $D_4$-B (see Supporting Information).

According to our newly established homology models, two amino acids preceding and following the disulfide forming cysteine residue of EL2 were expected to be involved in ligand binding. To investigate the influence of these

residues in $D_2/D_3$ selectivity, we decided to create both the $D_2$E181V+I183S and the $D_3$V180E+S182I double mutants. In fact, mutation of Val180 and Ser182 of the $D_3$ receptor into the corresponding amino acids present at the $D_2$ receptor (Glu and Ile, respectively) resulted in a 20-fold increase in binding affinity for the preferential $D_2$ ligand **2a** at the mutant $D_3$ receptor. Accordingly, the thio analogue **2b** displayed an 8-fold enhancement of affinity. The resulting $K_i$ values were comparable to those measured for both test compounds at the $D_2$ wild type. Interestingly, this mutation did not affect the affinity of the ligands **3a,b**. The reciprocal double mutation $D_2$E181V+I183S resulted in a 3-fold to 12-fold decrease in affinity of both the preferential $D_2$ (**2a,b**) and $D_3$ (**3a,b**) ligands.

Although the longer $D_3$ selective phenylpiperazines **3a,b** could not profit from the mutations at the $D_2$ receptor, these results confirm that Glu181/Ile183 at the $D_2$ and Val180/ Ser182 at the $D_3$ receptor are involved in $D_2/D_3$ subtype selectivity. In agreement with our ligand–receptor models (Figure 2), we assume that the mutation of Ser182 of the $D_3$ receptor into an isoleucine introduces a $D_2$-like hydrophobic binding region next to the conserved cysteine in EL2. This additional hydrophobicity is beneficial for high affinity binding of the azaindole moiety in the preferential $D_2$ ligands **2a,b**.

## Conclusions

Chemical synthesis of specific molecular probes and SAR studies combined with computational predictions and site directed mutagenesis proved to be a powerful tool facilitating the discovery of the structural origins of subtype selectivity. Homology modeling and ligand docking have significantly profited from the recent $\beta_2$-adrenergic receptor crystal structure and the inclusion of a carefully modeled EL2. We were able to further examine amino acids present at position 2.61 in TM2 and positions 3.28 and 3.29 in TM3 and their importance in $D_4/D_2$ and $D_3/D_4$ receptor subtype selectivity. Mutagenesis of Asp[3.32] and His[6.55] revealed that, in spite of their conservation, the residues contribute differently to ligand binding at the subtypes $D_2$ and $D_3$. Thus, differences in interhelical interfaces can lead to distortions in the spatial arrangement of the ligand binding pocket mediated by conserved residues like His[6.55]. Careful modeling of the extracellular loop 2 revealed Glu181/Val180 and Ile183/Ser182 to be involved in ligand binding and selectivity of the $D_2$ and $D_3$ receptor, together with the critical residues 2.61, 2.64, 3.28, and 3.29. These results could be corroborated by site directed mutagenesis, thereby validating our ligand–receptor complexes and showing the importance of these residues in $D_2/D_3$ selectivity. Interactive processes between computational predictions and experimental validation will guide new experiments that further elucidate the molecular origins of subtype specificity and a general rational design of subtype selective GPCR ligands.

## Experimental Section

**Chemistry.** All reactions were carried out under nitrogen atmosphere. Dry solvents and reagents were commercial quality and used as purchased. MS were run on a Finnigan MAT TSQ 700 spectrometer by EI (70 eV) with solid inlet or with an ion-trap mass with APCI ionization. HR-EIMS were run on a Finnigan MAT 8200 using peak Peak-Matching ($M/\Delta M$ = 10 000). NMR spectra were obtained on a Bruker Avance 360 or a Bruker Avance 600 spectrometer relative to TMS in the solvents indicated ($J$ values in Hz). IR spectra were performed on a Jasco FT/IR 410 spectrometer using a film of substance on a NaCl pill. Purification by flash chromatography was performed using silica gel 60 if not stated otherwise. TLC analyses were performed using Merck 60 F254 aluminum sheets and analyzed by UV light (254 nm) or by spraying with ninhydrin reagent. Analytical HPLC/MS was performed on Agilent 1100 HPLC systems employing a VWL detector connected to a Bruker Esquire 2000. The purity of all SAR compounds was determined to be >95% by reverse phase HPLC. As column, a Zorbax SB-C18 (4.6 mm i.d. × 150 mm, 5 $\mu$m) with a flow rate of 0.5 mL/min was used (eluent, methanol/water/0.1 N formic acid, 10% methanol for 3 min to 100% methanol in 15 min, 100% for 6 min to 10% in 3 min, 10% for 3 min). Compound **1b** was further checked for its purity via combustion analysis on a EA 1110 CHNS (CE) instrument performed at the Chair of Organic Chemistry, Friedrich-Alexander-Universitat, Erlangen-Nurnberg.

**3-[4-(2-Methylsulfanylphenyl)piperazin-1-yl]propionitrile (5).** 1-(2-Methylsulfanylphenyl)piperazine (744 mg, 3.15 mmol), $K_2CO_3$ (1000 mg, 7.26 mmol), and NaI (88.9 mg, 0.59 mmol) were dissolved in $CH_3CN$ (20.0 mL). 3-Bromopropionitrile (559 mg, 4.17 mmol) was added, and the mixture was heated to reflux for 24 h. The solvent was removed under reduced pressure and the resulting residue was purified using flash chromatography (hexane/EtOAc 1:1) to give **5** (554 mg, 67% related to 1-(2-methylsulfanylphenyl)piperazine as white crystalline solid. Mp: 88 °C. IR $\nu$ 3054, 2942, 2919, 2878, 2819, 2683, 2247, 1579, 1472, 1440 cm$^{-1}$. $^1$H NMR (CDCl$_3$, 600 MHz) $\delta$ 2.41 (s, 3H), 2.56 (t, $J = 7.2$, 2H), 2.65–2.74 (m, 4H), 2.78 (t, $J = 7.0$, 2H), 2.99–3.07 (m, 4H), 7.03–7.07 (m, 1H), 7.09–7.14 (m, 3H). $^{13}$C NMR (CDCl$_3$, 90 MHz) $\delta$ 14.3, 15.9, 51.4, 53.0, 53.4, 118.8, 119.6, 124.2, 124.6, 124.9, 135.0, 149.2. HPLC/MS (254 nm) purity >99% ($t_R$ = 14.0 min). APCI-MS, [M + H]$^+$: calcd, 261.1; found, 262.0. EI-MS: $m/z$ 261 (M$^+$). HR-EIMS: calcd, 261.1300; found, 261.1300.

**3-[4-(2-Methylsulfanylphenyl)piperazin-1-yl]propylamine (6).**[30,31] 3-[4-(2-Methylsulfanylphenyl)piperazin-1-yl]propionitrile (100 mg, 0.35 mmol) was dissolved in dry Et$_2$O (4.0 mL) and cooled to −5 to 0 °C. LiAlH$_4$ (1 M in Et$_2$O, 0.83 mL, 0.83 mmol) was added, and the solution was stirred at room temperature for 1 h. After being cooled to 0 °C, the solution was quenched with a saturated solution of NaHCO$_3$. The solution was stirred with MgSO$_4$ and filtered through a short column of Celite and MgSO$_4$. The filtrate was evaporated under reduced pressure to give **6** (18.2 mg, 18%) as light-brown oil. IR $\nu$ 3353, 3281, 3055, 2941, 2876, 2816, 2680, 2184, 1579, 1472, 1440 cm$^{-1}$. $^1$H NMR (CDCl$_3$, 360 MHz) $\delta$ 1.69 (tt, $J = 7.0$, 7.1, 2H), 2.41 (s, 3H, CH$_3$), 2.49 (t, $J = 7.4$, 2H), 2.49–2.72 (m, 4H), 2.78 (t, $J = 6.8$, 2H), 2.99–3.11 (m, 4H), 7.02–7.16 (m, 4H). $^{13}$C NMR (CDCl$_3$, 90 MHz) $\delta$ 14.4, 30.7, 40.9, 46.5, 51.7 (2C), 53.8 (2C), 56.6, 119.6, 124.2, 124.4, 124.9, 135.0, 149.5. HR-EIMS: calcd, 265.1613; found, 265.1613.

**N-[3-[4-(2-Methylsulfanylphenyl)piperazin-1-yl]propyl]pyrazolo-[1,5-a]pyridine-3-carboxamide (2b).** Pyrazolo[1,5-a]pyridine-3-carboxylic acid (11.0 mg, 0.068 mmol) was dissolved in dry CH$_2$Cl$_2$ (2.2 mL) under nitrogen, and DIPEA (0.04 mL, 0.02 mmol) was added. The mixture was cooled to 0 °C while stirring. A solution of TBTU (21.4 mg, 0.067 mmol) in DMF (0.2 mL) was then added dropwise to the cooled reaction mixture. The mixture was allowed to reach room temperature. 3-[4-(2-Methylsulfanylphenyl)piperazin-1-yl]propylamine (**6**) (18.0 mg, 0.068 mmol) dissolved in CH$_2$Cl$_2$ was added dropwise at room temperature, and stirring was continued for 2 h. The mixture was then washed with a saturated aqueous solution of NaHCO$_3$. The layers were separated, and the aqueous layer was extracted with CH$_2$Cl$_2$. The combined organic layers were then washed with brine, dried over Na$_2$SO$_4$, filtered, and evaporated. Purification using flash chromatography with CH$_2$Cl$_2$/MeOH, 95:5, revealed **2b** (24 mg, 87% related to **6**) as a light-brown foam. Mp: 75–80 °C. IR $\nu$ 3314, 2922, 2816, 2233, 1638, 1552, 1530 cm$^{-1}$. $^1$H NMR (CDCl$_3$,

360 MHz) δ 1.89 (tt, $J$ = 6.0, 6.0, 2H), 2.41 (s, 3H), 2.70 (t, $J$ = 6.0, 2H), 2.62−2.86 (m, 4H), 3.04−3.16 (m, 4H), 3.62 (dt, $J$ = 5.7, 5.8, 2H), 6.90 (ddd, $J$ = 6.8, 7.5, 1.1, 1H), 7.05−7.17 (m, 4H), 7.33 (ddd, $J$ = 8.9, 6.8, 1.1, 1H), 7.66 (br s, 1H), 8.29 (s, 1H), 8.34 (ddd, $J$ = 8.9, 1.1, 1.1, 1H), 8.48 (ddd, $J$ = 6.9, 1.0, 0.9, 1H). $^{13}$C NMR (CDCl$_3$, 90 MHz) δ 13.3, 23.8, 38.5, 50.4, 52.8, 57.0, 106.2, 112.4, 118.7, 118.7, 123.3, 123.7, 124.0, 125.1, 127.8, 133.9, 139.5, 139.6, 147.9, 162.4. HPLC/MS (254 nm) purity 99% ($t_R$ = 15.8 min). APCI-MS, [M + H]$^+$: calcd, 409.6; found:, 410.2. EI-MS: $m/z$ 409 (M$^+$). HR-EIMS: calcd, 409.1937; found, 409.1936.

**Methyl 2-(4-Ethoxycarbonylbutyl)pyrazolo[1,5-*a*]pyridine-3-carboxylate (8).** The reaction was carried out using 1-aminopyridinium iodide (3.0 g, 13.5 mmol), K$_2$CO$_3$ (1.5 g, 11 mmol), and 3-oxooctanedioic acid 8-ethyl ester 1-methyl ester (**7**) (3.3 g, 14.3 mmol) in DMF (10 mL) and stirred at 50 °C for 2 h.$^{32−35}$ After addition of saturated NaHCO$_3$ solution, the mixture was extracted with Et$_2$O and washed with water. The organic solvent was dried over MgSO$_4$ and evaporated. The crude product was purified by flash chromatography (hexane/EtOAc, 8:2) yielding **8** as a solid (0.5 g, 13%). Mp: 46 °C. IR $v$ 2980, 2950, 2872, 1732, 1703, 1636, 1519, 1095 cm$^{-1}$. $^1$H NMR (CDCl$_3$, 360 MHz) δ 1.24 (t, $J$ = 7.1, 3H), 1.71−1.89 (m, 4H), 2.35−2.39 (m, 2H), 3.10−3.14 (m, 2H), 3.92 (s, 3H), 4.12 (q, $J$ = 7.1, 2H), 6.89 (ddd, $J$ = 7.1, 6.7, 1.4, 1H), 7.36 (ddd, $J$ = 8.9, 6.7, 1.1, 1H), 8.09 (br d, $J$ = 8.9, 1H), 8.43 (dd, $J$ = 7.1, 1.1, 1H). $^{13}$C NMR (CDCl$_3$, 90 MHz) δ 14.2, 24.9, 27.8, 28.5, 34.2, 50.9, 60.2, 100.5, 113.2, 119.1, 127.1, 128.7, 142.2, 159.2, 173.7, 164.3. EI-MS: $m/z$ 304 (M$^+$). Anal. Calcd for C$_{16}$H$_{20}$N$_2$O$_4$: C, 63.14; H, 6.62; N, 9.20. Found: C, 63.24; H, 6.75; N, 8.83.

**5-(Pyrazolo[1,5-*a*]pyridine-2-yl)pentanoic Acid (9).** A suspension of **8** (400 mg, 1.31 mmol) in 40% H$_2$SO$_4$ solution (13 mL) was stirred at 110 °C for 3 h. After cooling to room temperature, the solution was neutralized with NaOH (5 M), and HCl (2 M) was added to get pH 3. Extraction with CHCl$_3$ gave a white solid of compound **9** (255 mg, 93%). Mp: 121 °C. IR $v$ 3522, 2944, 2869, 1709, 1635 cm$^{-1}$. $^1$H NMR (DMSO, 360 MHz) δ 1.54−1.60 (m, 2H), 1.65−1.72 (m, 2H), 2.25 (t, $J$ = 7.1, 2H), 2.73 (t, $J$ = 7.1, 2H), 6.38 (s, 1H), 6.77 (ddd, $J$ = 7.1, 6.7, 1.4, 1H), 7.13 (ddd, $J$ = 8.9, 6.7, 1.1, 1H), 7.56 (br d, $J$ = 8.9, 1H), 8.55 (dd, $J$ = 7.1, 1.1, 1H), 11.98 (s, 1H). $^{13}$C NMR (DMSO, 90 MHz) δ 24.2, 27.6, 28.5, 33.4, 94.0, 111.0, 117.2, 123.3, 128.3, 140.3, 155.0, 174.4. EI-MS: $m/z$ 218 (M$^+$).

**1-[4-(4-Chlorophenyl)piperazin-1-yl]-5-[pyrazolo[1,5-*a*]pyridin-2-yl]pentan-1-one (10).** The reaction was carried out using **9** (218 mg, 1.0 mmol), HOAt (150 mg, 1.1 mmol), DCC (227 mg, 1.1 mmol), and 4-chlorophenylpiperazine (236 mg, 1.2 mmol) in CH$_2$Cl$_2$ (10 mL) under nitrogen atmosphere. The mixture was stirred at room temperature for 15 h and filtered, and the solvent was evaporated. The crude product was purified by flash chromatography (CH$_2$Cl$_2$/MeOH, 98:2), obtaining a white solid of **10** (322 mg, 81%). Mp: 117 °C. IR $v$ 2930, 2857, 2826, 1644, 1635, 1231, 1029 cm$^{-1}$. $^1$H NMR (CDCl$_3$, 360 MHz) δ 1.70−1.86 (m, 4H), 2.39−2.43 (m, 2H), 2.84−2.89 (m, 2H), 3.05−3.10 (m, 4H), 3.56−3.59 (m, 2H), 3.73−3.77 (m, 2H), 6.30 (s, 1H), 6.65 (br dd, $J$ = 7.1, 6.7, 1H), 6.79−6.83 (m, 2H), 7.03 (brdd, $J$ = 8.9, 6.7, 1H), 7.19−7.24 (m, 2H), 7.40 (br d, $J$ = 8.9, 1H), 8.34 (br d, $J$ = 7.1, 1H). $^{13}$C NMR: (CDCl$_3$, 90 MHz) δ 24.9, 28.1, 29.3, 33.0, 41.3, 45.4, 49.4, 49.7, 95.2, 110.8, 117.4, 117.8, 123.1, 125.4, 128.1, 129.1, 141.0, 149.6, 155.8, 171.5. EI-MS: $m/z$ 396 (M$^+$). Anal. Calcd for C$_{22}$H$_{25}$N$_4$OCl: C, 66.57; H, 6.35; N, 14.12. Found: C, 66.52; H, 6.49; N, 13.93.

**2-[5-[4-(4-Chlorophenyl)piperazin-1-yl]pentyl]pyrazolo[1,5-*a*]-pyridine (1b).** A suspension of **10** in dry, absolute Et$_2$O was treated with 1.0 M LiAlH$_4$ solution in Et$_2$O (2 equiv) and stirred under nitrogen atmosphere at 0 °C for 1 h and subsequently at room temperature for 5 h. Saturated NaHCO$_3$ solution was added dropwise to quench the remaining LiAlH$_4$. The mixture was filtered on Celite and washed with MeOH. The crude product was purified by flash chromatography (CH$_2$Cl$_2$/MeOH 98:2) to obtain a white solid of **1b** (114 mg, 59%). Mp: 72 °C.

IR $v$ 2936, 2860, 2816, 1634, 1496, 1235 cm$^{-1}$. $^1$H NMR (CDCl$_3$, 360 MHz) δ 1.40−1.49 (m, 2H), 1.55−1.63 (m, 2H), 1.75−1.84 (m, 2H), 2.37−2.41 (m, 2H), 2.56−2.59 (m, 4H), 2.81−2.85 (m, 2H), 3.14−3.17 (m, 4H), 6.28 (s, 1H), 6.65 (brdd, $J$ = 7.1, $J$ = 6.7, 1H), 6.81−6.85 (m, 2H), 7.04 (brdd, $J$ = 8.9, 6.7, 1H), 7.17−7.21 (m, 2H), 7.41 (brd, $J$ = 8.9, 1H), 8.37 (brd, $J$ = 7.1, 1H). $^{13}$C NMR (CDCl$_3$, 90 MHz) δ 26.7, 27.4, 28.5, 29.7, 49.1, 53.1, 58.6, 95.1, 110.8, 117.1, 117.3, 123.1, 124.3, 128.2, 128.9, 141.0, 150.0, 156.2. EI-MS: $m/z$ 382 (M$^+$), 384 (M$^+$ + 2). Anal. Calcd for C$_{22}$H$_{27}$N$_4$Cl·0.6H$_2$O: C, 67.11; H, 7.22; N, 14.23. Found: C, 67.62; H, 7.22; N, 13.72.

**Residue Numbering Scheme.** For reasons of clarity, amino acid positions are numbered according to Ballesteros and Weinstein. Residues are numbered consecutively as [TM$x$].$n$ relative to the most conserved residue within each TM, which is designated as [TM$x$].50.$^{55}$

**Dopamine Receptor Binding Studies.** Receptor binding studies were carried out as described.$^{56}$ In brief, competition experiments with human D$_{2L}$, D$_3$, and D$_4$ receptors were run with preparations of membranes from CHO cells stably expressing the corresponding receptor and [$^3$H]spiperone at a final concentration of 0.1−0.3 nM according to the individual $K_d$ values. The assays were carried out with a protein concentration of 5−20 $\mu$g/assay tube and $K_d$ values of 0.06−0.14, 0.08−0.35, and 0.15−0.40 nM for the D$_{2L}$, D$_3$, and D$_4$ receptors, respectively. The corresponding $B_{max}$ values were in the range of 750−1400 fmol/mg for D$_{2L}$, 1500−4300 fmol/mg for D3, and 700−1800 fmol/mg for D$_4$, respectively. Protein concentration was established by the method of Lowry using bovine serum albumin as standard.$^{57}$

**Data Analysis.** The resulting competition curves of the receptor binding experiments were analyzed by nonlinear regression using the algorithms in PRISM 3.0 (GraphPad Software, San Diego, CA). The data were initially fit using a sigmoid model to provide a slope coefficient ($n_H$) and an IC$_{50}$ value, representing the concentration corresponding to 50% of maximal displacement of the radioligand. The IC$_{50}$ values were transformed to $K_i$ values according to the equation of Cheng and Prusoff.$^{58}$

**Site Directed Mutagenesis.** The hDRD2 cDNA, subcloned into a pcDNA3.1(+) eukaryotic expression vector, was purchased from UMR cDNA Resource Center. The pcDNA3.1(+) of hDRD3 receptor and of the hDRD$_{4.4}$ were used as described previously.$^{53}$ Oligonucleotidic primers were purchased from Biomers.net or MWG Biotech AG. Site directed mutagenesis was performed by polymerase chain reaction (PCR) using oligonucleotides bearing the desired mutation.$^{59}$ Fidelity of PCR amplification and introduction of mutations in the receptor cDNA was confirmed by sequencing with the ABI sequencer system (ABI Systems, Weiterstadt, Germany) at the laboratory of C.-M. Becker (Department of Biochemistry, FAU Erlangen, Germany) using oligonucleotidic primers.

**Mutant Receptor Preparation.** HEK-293 cells, transiently transfected with the wildtype and mutant receptor cDNA by CaHPO$_4$ method or using TransIT-293 transfection reagent (Mirus Bio Corporation), were cultured in 150 mm Petri plates containing 20 mL of MEM α medium supplemented with 10% (v/v) fetal bovine serum, 100 U/mL penicillin G, 100 $\mu$g/mL streptomycin, and 2 mM L-glutamine at 37 °C and 5% CO$_2$.

HEK-293 cells were harvested 48 h after transfection. Cells were harvested by removal of the medium, followed by a wash with phosphate buffered saline, which was discarded, resuspension in 10 mL of harvest puffer (10 mM Tris-HCl, 0.5 mM EDTA, 5.4 mM KCl, and 140 mM NaCl, pH 7.4), scraping of the cells with a rubber spatula into a centrifuge tube, and collection of the cells by centrifugation at 220$g$ for 8 min. The cellular pellet was resuspended in 5 mL of homogenate buffer for D$_2$ and D$_4$ receptor (50 mM Tris-HCl, 5 mM EDTA, 1,5 mM CaCl$_2$, 5 mM MgCl$_2$, 5 mM KCl, and 120 mM NaCl, pH 7,4)

and for $D_3$ receptor (10 mM Tris-HCl and 5 mM MgSO$_4$, pH 7,4). Cells were used as they were or stored at −80 °C.

After thawing or directly, the cells were diluted in homogenate buffer, homogenized using a Polytron (20 000 rpm, 5 × 5 s each in an ice bath), and spun at 50000$g$ for 18 min. The membrane pellet was always resuspended in homogenate puffer for $D_2$ and $D_4$ receptor, homogenized with a Potter−Elvehjem homogenizer, and stored in small aliquots at −80 °C. Protein concentration was estimated by the method of Lowry et al., using bovine serum albumin as a standard.[57]

**Radioligand Binding Studies.** The radioligand [$^3$H]spiperone was purchased from Amersham/GE Healthcare UK Limited and obtained with a specific activity of 84−114 Ci/mmol. $K_D$ and $B_{max}$ values for wild type and mutants were received from saturation experiments, and the $K_i$ values for the compounds were obtained by competition experiments.

The competition binding assay followed the previously published protocol.[56] In brief, binding assays with $D_2$, $D_3$, and $D_{4.4}$ wild type and mutant receptors were performed with [$^3$H]spiperone at the final concentrations of 0.1−0.7 nM. The assays were carried out in the 96-well plates at the protein concentration of 20−200 $\mu$g/mL in a final volume of 200 $\mu$L. $K_i$ values were derived from the corresponding EC$_{50}$ data.[58]

**Dopamine Receptor Modeling.** The crystal structure of the human $\beta_2$-adrenergic receptor (PDB entry 2RH1) was used as a template to construct the dopaminergic receptors.[37] The amino acid sequences of the human dopamine $D_2$, $D_3$, and $D_4$ receptors and the $\beta_2$-adrenergic receptor were retrieved from the SWISS-PROT database.[60] Sequence alignment was performed by means of ClustalX by employing the Gonnet series matrix with a gap open penalty of 10 and a gap extension penalty of 0.2.[61] To define highly conserved residues, 10 additional sequences of members of the family A GPCRs were included in the alignment that was manually refined to ensure a perfect alignment of the highly conserved residues of the GPCR superfamily according to Baldwin et al.[62]

On the basis of the alignment and the crystal structure of the $\beta_2$-adrenergic receptor, 100 models of each receptor ($D_2$, $D_3$, and $D_4$) were constructed using the MODELLER program.[63] The extracellular loop 2 (EL2) was omitted because of the difference in sequence length between the dopaminergic receptors and the $\beta_2$-adrenergic receptor. The intracellular loop 3 is already absent in the crystal structure and omitted in receptor modeling.

One model was selected for each of the $D_2$ and $D_3$ receptor. For the $D_4$ receptor, two diverse models showing different $\chi_1$ rotamers at Phe$^{2.61}$ were selected by docking the $D_4$ ligand **1d** into each of the initial 100 model structures and subsequent scoring with DrugScore$^{ONLINE}$.[28,42] Further validation was achieved by additionally docking **1a** into these two $D_4$ receptor models.

**Modeling of the Extracellular Loop 2.** A prototype of the extracellular loop 2 (EL2) was modeled into the $D_4$ receptor model using the crystal structure of the $\beta_2$-adrenergic receptor, the loop database of the Swiss-PdbViewer, and molecular dynamics simulations by means of the SANDER program of the AMBER10 suite.[41,64]

Because of the similarity in sequence length, the crystal structure of the $\beta_2$-adrenergic receptor was used to model the EL2 ranging from the conserved cysteine, which forms a disulfide bond with Cys$^{3.25}$ in TM3, to the extracellular end of TM5 (position 5.36). The relevant amino acids were mutated using Swiss-PdbViewer. Because of a big difference in sequence length between the $\beta_2$-adrenergic and the dopamine receptors, the part of the EL2 ranging from the extracellular end of TM4 (position 4.61) to the conserved cysteine was modeled using the loop database of the Swiss-PdbViewer.

The receptor was then submitted to energy minimization in complex with the best docking solution of compound **1d**. The SANDER classic module of AMBER10 was used by applying

500 cycles of steepest descent minimization, followed by 4500 cycles of conjugate gradient minimization. All calculations were carried out in a water box with periodic boundary conditions and a nonbonded cutoff of 8.0 Å. The all atom force field ff99SB was applied.[65] Parameterization of **1d** was accomplished with antechamber. The charges for the ligand atoms were calculated using Gaussian 98, with a 6-31** basis set, and then the RESP procedure was applied as described in the literature.[66,67] A formal charge of +1 was attributed to the ligand because the piperazine nitrogen connected to the aliphatic chain is assumed to be protonated at physiological pH.

In the next step the minimized structure was submitted to MD simulations. By application of Shake bond-length restraints to bonds involving hydrogens, it was possible to set the time step to 2 fs. Nonbonded interactions were updated every 25 fs. The system was gradually heated to 300 K and equilibrated for 10 ns with a harmonic force constant of 1.0 kcal mol$^{-1}$ Å$^{-2}$ on the main chain atoms of the protein except EL2. Then 20 ns of MD simulations without restraints followed. The resulting final structure of EL2 was inserted into the original D4 receptor model using Swiss-PdbViewer.

Because of the same sequence length, part of this EL2, ranging from the conserved cysteine to the extracellular end of TM5 (position 5.36), was also used to construct the EL2 of the $D_2$ and the $D_3$ receptors. Nonconserved amino acids were mutated using Swiss-PdbViewer. Because of big differences in sequence length between the $D_4$ and the $D_2$ and $D_3$ receptors, the part of the EL2 ranging from the extracellular end of TM4 (position 4.61) to the conserved cysteine was modeled using the loop database of the Swiss-PdbViewer.

**Docking Procedure.** **1a**, **2b**, and **3a** were geometry optimized by means of Gaussian 98 at the 6-31** level, attributing a formal charge of +1 to all ligands. The ligands were then docked using the program AUTODOCK4.[68−70] A grid of 70 points in each of the $x$, $y$, and $z$ directions was used to completely enclose the binding pocket surrounded by the extracellular parts of TM2, TM3, TM5, TM6, and TM7. A grid spacing of 0.375 Å was used, and all ligands were subjected to 50 runs of the AUTODOCK Lamarckian genetic algorithm with a randomly selected starting position. The docking procedure was free of constraints, thereby exploring all the available grid space. The 50 docking conformations of each compound were clustered manually and scored by DrugScore$^{ONLINE}$ (www.agklebe.de), applying the knowledge-based DrugScore$^{CSD}$ scoring function.[42] On the basis of this scoring, the best conformation of each cluster was selected. After a final selection according to experimental data, the receptor−ligand complexes were subjected to energy minimization. Parametrization of the ligands, calculation of charges, and energy minimization were accomplished as described above.

**Supporting Information Available:** NMR spectra, LC/MS purity data including MS spectra, used oligonucleotide primer sequences, amino acid sequence alignment, and scoring results. This material is available free of charge via the Internet at http://pubs.acs.org. Described ligand−receptor complexes are available from the corresponding author upon personal request.

**References**

(1) Boeckler, F.; Lanig, H.; Gmeiner, P. Modeling the similarity and divergence of dopamin D2 like receptors and identification of

validated ligand−receptor complexes. *J. Med. Chem.* **2005**, *48*, 694–709.

(2) Salama, I.; Schlotter, K.; Utz, W.; Hubner, H.; Gmeiner, P.; Boeckler, F. CoMFA and CoMSIA investigations of dopamine D3 receptor ligands leading to the prediction, synthesis and evaluation of rigidized FAUC 365 analogues. *Bioorg. Med. Chem.* **2006**, *14*, 5898–5912.

(3) Pilla, M.; Perachon, S.; Sautel, F.; Garrido, F.; Mann, A.; Wermuth, C. G.; Schwartz, J.-C.; Everitt, B. J.; Sokoloff, P. Selective inhibition of cocaine-seeking behaviour by a partial dopamine D3 receptor agonist. *Nature* **1999**, *400*, 371–375.

(4) Boeckler, F.; Gmeiner, P. The structural evolution of dopamine D3 receptor ligands. Structure−activity relationships and selected neuropharmacological aspects. *Pharmacol. Ther*. **2006**, *112*, 281–333.

(5) Lober, S.; Tschammer, N.; Hubner, H.; Melis, M. R.; Argiolas, A.; Gmeiner, P. The azulene framework as a novel arene bioisostere: design of potent dopamine D4 receptor ligands inducing penile erection. *ChemMedChem* **2009**, *4*, 325–328.

(6) Enguehard-Gueiffier, C.; Hubner, H.; El Hakmaoui, A.; Allouchi, H.; Gmeiner, P.; Argiolas, A.; Melis, M. R.; Gueiffier, A. 2-[(4-Phenylpiperazin-1-yl)methyl]imidazo(di)azines as selective D4-ligands. Induction of penile erection by 2-[4-(2-methoxyphenyl)piperazin-1-ylmethyl]imidazo[1,2-*a*]pyridine (PIP3EA), a potent and selective D4 partial agonist. *J. Med. Chem.* **2006**, *49*, 3938–3947.

(7) Brioni, J. D.; Moreland, R. B.; Cowart, M.; Hsieh, G. C.; Stewart, A. O.; Hedlund, P.; Donnelly-Roberts, D. L.; Nakane, M.; Lynch, J. J.III; Kolasa, T.; Polakowski, J. S.; Osinski, M. A.; Marsh, K.; Andersson, K.-E.; Sullivan, J. P. Activation of dopamine D4 receptors by ABT-724 induces penile erection in rats. *Proc. Natl. Acad. Sci. U.S.A.* **2004**, *101*, 6758–6763.

(8) Ortore, G.; Tuccinardi, T.; Bertini, S.; Martinelli, A. A theoretical study to investigate D2DAR/D4DAR selectivity: receptor modeling and molecular docking of dopaminergic ligands. *J. Med. Chem.* **2006**, *49*, 1397–1407.

(9) Simpson, M. M.; Ballesteros, J. A.; Chiappa, V.; Chen, J.; Suehiro, M.; Hartman, D. S.; Godel, T.; Snyder, L. A.; Sakmar, T. P.; Javitch, J. A. Dopamine D4/D2 receptor selectivity is determined by a divergent aromatic microdomain contained within the second, third, and seventh membrane-spanning segments. *Mol. Pharmacol.* **1999**, *56*, 1116–1126.

(10) Kortagere, S.; Gmeiner, P.; Weinstein, H.; Schetz, J. A. Certain 1,4-disubstituted aromatic piperidines and piperazines with extreme selectivity for the dopamine D4 receptor interact with a common receptor microdomain. *Mol. Pharmacol.* **2004**, *66*, 1491–1499.

(11) Floresca, C. Z.; Chen, S.; Kortagere, S.; Schetz, J. A. Reciprocal mutations in TM2/TM3 in a D2 dopamine receptor background confirms the importance of this microdomain as a selective determinant of para-halogenated 1,4-disubstituted aromatic piperazines. *Arch. Pharm. (Weinheim, Ger.)* **2005**, *338*, 268–275.

(12) Lanig, H.; Utz, W.; Gmeiner, P. Comparative molecular field analysis of dopamine D4 receptor antagonists including 3-[4-(4-chlorophenyl)piperazin-1-ylmethyl]pyrazol[1,5-a]pyridine (FAUC 113), 3-[4-(4-chlorophenyl)piperazin-1-ylmethyl]-1*H*-pyrrolo-[2,3-*b*]pyridine (L-745,870), and clozapine. *J. Med. Chem.* **2001**, *44*, 1151–1157.

(13) Salama, I.; Hocke, C.; Utz, W.; Prante, O.; Boeckler, F.; Hubner, H.; Kuwert, T.; Gmeiner, P. Structure−selectivity investigations of D2-like receptor ligands by CoMFA and CoMSIA guiding the discovery of D3 selective PET radioligands. *J. Med. Chem.* **2007**, *50*, 489–500.

(14) Boeckler, F.; Ohnmacht, U.; Lehmann, T.; Utz, W.; Hubner, H.; Gmeiner, P. CoMFA and CoMSIA investigations revealing novel insights into the binding modes of dopamine D3 receptor agonists. *J. Med. Chem.* **2005**, *48*, 2493–2508.

(15) Wilcox, R. E.; Huang, W. H.; Brusniak, M. Y.; Wilcox, D. M.; Pearlman, R. S.; Teeter, M.; DuRand, C. J.; Wiens, B. L.; Neve, K. A. CoMFA-based prediction of agonist affinities at recombinant wild type versus serine to alanine point mutated D2 dopamine receptors. *J. Med. Chem.* **2000**, *43*, 3005–3019.

(16) Ravina, E.; Negreira, J.; Cid, J.; Masaguer, C. F.; Rosa, E.; Rivas, M. E.; Fontenla, J. A.; Loza, M. I.; Tristan, H.; Cadavid, M. I.; Sanz, F.; Lozoya, E.; Carotti, A.; Carrieri, A. Conformationally constrained butyrophenones with mixed dopaminergic (D(2)) and serotoninergic (5-HT(2A), 5-HT(2C)) affinities: synthesis, pharmacology, 3D-QSAR, and molecular modeling of (aminoalkyl)benzo- and -thienocycloalkanones as putative atypical antipsychotics. *J. Med. Chem.* **1999**, *42*, 2774–2797.

(17) Hackling, A.; Ghosh, R.; Perachon, S.; Mann, A.; Holtje, H. D.; Wermuth, C. G.; Schwartz, J. C.; Sippl, W.; Sokoloff, P.; Stark, H. *N*-(omega-(4-(2-Methoxyphenyl)piperazin-1-yl)alkyl)carboxamides as

dopamine D2 and D3 receptor ligands. *J. Med. Chem.* **2003**, *46*, 3883–3899.

(18) Cha, M. Y.; Lee, I. Y.; Cha, J. H.; Choi, K. I.; Cho, Y. S.; Koh, H. Y.; Pae, A. N. QSAR studies on piperazinylalkylisoxazole analogues selectively acting on dopamine D3 receptor by HQSAR and CoMFA. *Bioorg. Med. Chem.* **2003**, *11*, 1293–1298.

(19) Bostrom, J.; Bohm, M.; Gundertofte, K.; Klebe, G. A 3D QSAR study on a set of dopamine D4 receptor antagonists. *J. Chem. Inf. Comput. Sci.* **2003**, *43*, 1020–1027.

(20) Rodriguez Loaiza, P.; Lober, S.; Hubner, H.; Gmeiner, P. Click chemistry on solid phase: parallel synthesis of *N*-benzyltriazole carboxamides as super-potent G-protein coupled receptor ligands. *J. Comb. Chem.* **2006**, *8*, 252–261.

(21) Temple, D. L., Jr.; Lobeck, W. G., Jr. Phenoxyethyl-1,2,4,-triazol-3-one Antidepressants. US4338317, **1982**.

(22) Horton, D. A.; Bourne, G. T.; Smythe, M. L. The combinatorial synthesis of bicyclic privileged structures or privileged substructures. *Chem. Rev.* **2003**, *103*, 893–930.

(23) Heinrich, T.; Bottcher, H.; Gericke, R.; Baroszyk, G. D.; Anzali, S.; Seyfried, C. A.; Greiner, H. E.; van Amsterdam, C. Synthesis and structure−activity relationship in a class of indolebutylpiperazines as dual 5-HT1A receptor agonists and serotonin reuptake inhibitors. *J. Med. Chem.* **2004**, *47*, 4684–4692.

(24) Foguet, R.; Ortiz, J. A.; Gubert, S.; Raga, M. M.; Sacristan, A. Derivatives of Piperazine, Method for Making the Same. US4883797, **1989**.

(25) Lober, S.; Hubner, H.; Utz, W.; Gmeiner, P. Rationally based efficacy tuning of selective dopamine D4 receptor ligands leading to the complete antagonist 2-[4-(4-chlorophenyl)piperazin-1-ylmethyl]pyrazolo[1,5-a]pyridine (FAUC 213). *J. Med. Chem.* **2001**, *44*, 2691–2694.

(26) Bettinetti, L.; Schlotter, K.; Hubner, H.; Gmeiner, P. Interactive SAR studies: rational discovery of super-potent and highly selective dopamine D3 receptor antagonists and partial agonists. *J. Med. Chem.* **2002**, *45*, 4594–4597.

(27) Boeckler, F.; Russig, H.; Zhang, W.; Lober, S.; Schetz, J.; Hubner, H.; Ferger, B.; Gmeiner, P.; Feldon, J. FAUC 213, a highly selective dopamine D4 receptor full antagonist, exhibits atypical antipsychotic properties in behavioural and neurochemical models of schizophrenia. *Psychopharmacology* **2004**, *175*, 7–17.

(28) Lober, S.; Hubner, H.; Gmeiner, P. Azaindole derivatives with high affinity for the dopamine D4 Receptor: synthesis, ligand binding studies and comparison of molecular electrostatic potential maps. *Bioorg. Med. Chem. Lett.* **1999**, *9*, 97–102.

(29) Rosenbaum, D. M.; Cherezov, V.; Hanson, M. A.; Rasmussen, S. G. F.; Thian, F. S.; Kobilka, T. S.; Choi, H.-J.; Yao, X.-J.; Weis, W. I.; Stevens, R. C.; Kobilka, B. K. GPCR engineering yields high-resolution structural insights into beta2-adrenergic receptor function. *Science* **2007**, *318*, 1266–1273.

(30) Steiner, G.; Lubisch, W.; Bach, A.; Emling, F.; Wicke, K.; Teschendorf, H.-J.; Behl, B.; Kerrigan, F.; Cheetham, S. Preparation of 3-substituted pyrido(4′,3′:4,5)thieno[2,3-*d*]pyrimidines as 5-HT1A receptor antagonists and serotonin reuptake inhibitors. *Ger. Offen.* **1998**, 8 pp.

(31) Steiner, G.; Schellhaas, K.; Lubisch, W.; Holzenkamp, U.; Starck, D.; Knopp, M.; Szabo, L.; Emling, F.; Garcia-Ladona, F. J.; Hofmann, H.-P.; Unger, L. Preparation of thienopyrimidines for use in the prophylaxis and therapy of cerebral ischemia. *Ger. Offen.* **2000**, 26 pp.

(32) Oikawa, Y.; Yoshioka, T.; Sugano, K.; Yonemitsu, O. Methyl phenylacetylacetate from phenylacetyl chloride and meldrum's acid. *Org. Synth.* **1985**, *63*, 198–202.

(33) Oikawa, Y.; Sugano, K.; Yonemitsu, O. Meldrum's acid in organic synthesis. 2. A general and versatile synthesis of .beta.-keto esters. *J. Org. Chem.* **1978**, *43*, 2087–2088.

(34) Thoma, H.; Spiteller, G. Meerwein-verseifung von 3-oxoalkansaure-alkylestern im gaschromatographen. *Liebigs Ann. Chem.* **1983**, 1237–1248.

(35) Goesl, R.; Meuwsen, A. 1-Aminopyridinium iodide. *Org. Synth.* **1963**, *43*, 1–3.

(36) Gmeiner, P.; Huebner, H.; Bettinetti, L.; Schlotter, K. Preparation of 2-Indolizinecarboxamides and Related Compounds as Central Nervous System Agents. WO 2006/015737, **2006**.

(37) Cherezov, V.; Rosenbaum, D. M.; Hanson, M. A.; Rasmussen, S. G. F.; Thian, F. S.; Kobilka, T. S.; Choi, H. J.; Kuhn, P.; Weis, W. I.; Kobilka, B. K.; Stevens, R. C. High-resolution cystal structure of an engineered human β2 adrenergic G protein-coupled receptor. *Science* **2007**, *318*, 1258–1265.

(38) van Leeuwen, D. H.; Eisensetin, J.; O'Malley, K.; MacKenzie, R. G. Characterization of a chimeric human dopamine D3/D2 receptor functionally coupled to adenylyl cyclase in Chinese hamster ovary cell. *Mol. Pharmacol.* **1995**, *48*, 344–351.

(39) Okada, T.; Sugihara, M.; Bondar, A. N.; Elstner, M.; Entel, P.; Buss, V. The retinal conformation and its environment in rhodopsin in light of a new 2.2 Å crystal structure. *J. Mol. Biol.* **2004**, *342*, 571–583.

(40) Shi, L.; Javitch, J. A. The second extracellular loop of the dopamine D2 receptor lines the binding-site crevice. *Proc. Natl. Acad. Sci. U. S.A.* **2004**, *101*, 440–445.

(41) Guex, N.; Peitsch, M. C. SWISS-MODEL and the Swiss-PdbViewer: an environment for comparative protein modeling. *Electrophoresis* **1997**, *18*, 2714–2723.

(42) Velec, H. F. G.; Gohlke, H.; Klebe, G. DrugScore$^{CSD}$-knowledge-based scoring function derived from small molecule crystal data with superior recognition rate of near-native ligand poses and better affinity prediction. *J. Med. Chem.* **2005**, *48*, 6296–6303.

(43) Mansour, A.; Meng, F.; Meador-Woodruff, J. H.; Taylor, L. P.; Civelli, O.; Akil, H. Site-directed mutagenesis of the human dopamine D$_2$ receptor. *Eur. J. Pharmacol.* **1992**, *227*, 205–214.

(44) Daniell, S. J.; Strange, P. G.; Naylor, L. H. Site-directed mutagenesis of Tyr417 in the rat D2 dopamine receptor. *Biochem. Soc. Trans.* **1994**, *22*, 144S.

(45) Cho, W.; Taylor, L. P.; Mansour, A.; Akil, H. Hydrophobic residues of the D2 dopamine receptor are important for binding and signal transduction. *J. Neurochem.* **1995**, *65*, 2105–2115.

(46) Shi, L.; Javitch, J. A. The binding site of aminergic G protein-coupled receptors: the transmembrane segments and second extracellular loop. *Annu. Rev. Pharmacol. Toxicol.* **2002**, *42*, 437–467.

(47) Warne, T.; Serrano-Vega, M. J.; Baker, J. G.; Moukhametzianov, R.; Edwards, P. C.; Henderson, R.; Leslie, A. G.; Tate, C. G.; Schertler, G. F. X. Structure of a beta1-adrenergic G-protein-coupled receptor. *Nature* **2008**, *454*, 486–491.

(48) Jaakola, V.-P.; Griffith, M. T.; Hanson, M. A.; Cherezov, V.; Chien, E. Y. T.; Lane, J. R.; Ijzerman, A. P.; Stevens, R. C. The 2.6 angstrom crystal structure of a human A$_{2A}$ adenosine receptor bound to an antagonist. *Science* **2008**, *322*, 1211–1217.

(49) Miller, D. D.; Harrold, M.; Wallace, R. A.; Wallace, L. J.; Uretsky, N. J. Dopaminergic drugs in the cationic form interact with D2 dopamine receptors. *Trends Pharmacol. Sci.* **1988**, *9*, 282–284.

(50) Woodward, R.; Daniell, S. J.; Strange, P. G.; Naylor, L. H. Structural studies on D2 dopamine receptors: mutation of a histidine residue specifically affects the binding of a subgroup of substituted benzamide drugs. *J. Neurochem.* **1994**, *62*, 1664–1669.

(51) Javitch, J. A.; Ballesteros, J. A.; Weinstein, H.; Chen, J. A cluster of aromatic residues in the sixth membrane-spanning segment of the dopamine D2 receptor is accessible in the binding-site crevice. *Biochemistry* **1998**, *37*, 998–1006.

(52) Lundstrom, K.; Turpin, M. P.; Large, C.; Robertson, G.; P., T.; Lewell, X.-Q. Mapping of dopamine D3 receptor binding site by pharmacological characterization of mutants expressed in CHO cells with the Semliki Forest virus system. *J. Recept. Signal Transduction Res.* **1998**, *18*, 133–150.

(53) Dorfler, M.; Tschammer, N.; Hamperl, K.; Hubner, H.; Gmeiner, P. Novel D3 selective dopaminergics incorporating enyne units as nonaromatic catechol bioisosteres: synthesis, bioactivity, and mutagenesis studies. *J. Med. Chem.* **2008**, *51*, 6829–6838.

(54) Bordo, D.; Argos, P. Suggestions for "safe" residue substitutions in site directed mutagenesis. *J. Mol. Biol.* **1991**, *217*, 721–729.

(55) Ballesteros, J.; Weinstein, H. Integrated Methods for the Construction of Three-Dimensional Models of Structure−Function Relations in G Protein-Coupled Receptors. In Methods in Neurosciences: Receptor Molecular Biology; Sealfon, S. C., Conn, M. P., Eds.; Academic Press: San Diego, CA, 1995; pp 366−428.

(56) Hubner, H.; Haubmann, C.; Utz, W.; Gmeiner, P. Conjugated enynes as nonaromatic catechol bioisosteres: synthesis, binding experiments, and computational studies of novel dopamine receptor agonists recognizing preferentially the D3 subtype. *J. Med. Chem.* **2000**, *43*, 756–762.

(57) Lowry, O. H.; Rosebrough, N. J.; Farr, A. L.; Randall, R. J. Protein measurement with the Folin phenol reagent. *J. Biol. Chem.* **1951**, *193*, 265–275.

(58) Cheng, Y.; Prusoff, W. H. Relationship between the inhibition constant (KI) and the concentration of inhibitor which causes 50% inhibition (I50) of an enzymatic reaction. *Biochem. Pharmacol.* **1973**, *22*, 3099–3108.

(59) Breitinger, H. C.; Villmann, C.; Becker, K.; Becker, C.-M. Opposing effects of molecular volume and charge at the hyperekplexia site 1(P250) govern glycine receptor activation and desensitization. *J. Biol. Chem.* **2001**, *276*, 29657–29663.

(60) Boeckmann, B.; Bairoch, A.; Apweiler, R.; Blatter, M. C.; Estreicher, A.; Gasteiger, E.; Martin, M. J.; Michoud, K.; O'Donovan, C.; Phan, I.; Pilbout, S.; Schneider, M. The SWISS-PROT protein knowledge-base and its supplement TrEMBL in 2003. *Nucleic Acids Res.* **2003**, *31*, 365–370.

(61) Thompson, J. D.; Gibson, T. J.; Plewniak, F.; Jeanmougin, F.; Higgins, D. G. The CLUSTAL_X windows interface: flexible strategies for multiple sequence alignment aided by quality analysis tools. *Nucleic Acids Res.* **1997**, *25*, 4876–4882.

(62) Baldwin, J. M.; Schertler, G. F. X.; Unger, V. M. An alpha-carbon template for the transmembrane helices in the rhodopsin family of G-protein-coupled receptors. *J. Mol. Biol.* **1997**, *272*, 144–164.

(63) Sali, A.; Blundell, T. L. Comparative protein modelling by satisfaction of spatial restraints. *J. Mol. Biol.* **1993**, *234*, 779–815.

(64) Case, D. A.; Darden, T. A.; Cheatham, T. E.; Simmerling, C. L.; Wang, J.; Duke, R. E.; Luo, R.; Crowley, M.; Walker, R. C.; Zhang, W.; Merz, K. M.; Wang, B.; Hayik, S.; Roitberg, A.; Seabra, G.; Kolossváry, I.; Wong, K. F.; Paesani, F.; Vanicek, J.; Wu, X.; Brozell, S. R.; Steinbrecher, T.; Gohlke, H.; Yang, L.; Tan, C.; Mongan, J.; Hornak, V.; Cui, G.; Mathews, D. H.; Seetin, M. G.; Sagui, C.; Babin, V.; Kollman, P. A. AMBER 10; University of California: San Francisco, 2008.

(65) Hornak, V.; Abel, R.; Okur, A.; Strockbine, B.; Roitberg, A.; Simmerling, C. Comparison of multiple amber force fields and development of improved protein backbone parameters. *Proteins: Struct., Funct., Bioinf.* **2006**, *65*, 712–725.

(66) Bayly, C. I.; Cieplak, W.; Kollman, P. A. A well-behaved electrostatic potential based method using charge restraints for determining atom-centered charges: the resp model. *J. Phys. Chem.* **1992**, *13*, 952–962.

(67) Frisch, M. J.; Trucks, G. W.; Schlegel, H. B.; Scuseria, G. E.; Robb, M. A.; Cheeseman, J. R.; Zakrzewski, V. G.; Montgomery, J. A., Jr.; Stratmann, R. E.; Burant, J. C.; Dapprich, S.; Millam, J. M.; Daniels, A. D.; Kudin, K. N.; Strain, M. C.; Farkas, O.; Tomasi, J.; Barone, V.; Cossi, M.; Cammi, R.; Mennucci, B.; Pomelli, C.; Adamo, C.; Clifford, S.; Ochterski, J.; Petersson, G. A.; Ayala, P. Y.; Cui, Q.; Morokuma, K.; Malick, D. K.; Rabuck, A. D.; Raghavachari, K.; Foresman, J. B.; Cioslowski, J.; Ortiz, J. V.; Stefanov, B. B.; Liu, G.; Liashenko, A.; Piskorz, P.; Komaromi, I.; Gomperts, R.; Martin, R. L.; Fox, D. J.; Keith, T.; Al-Laham, M. A.; Peng, C. Y.; Nanayakkara, A.; Gonzalez, C.; Challacombe, M.; Gill, P. M. W.; Johnson, B..; Chen, W.; Wong, M. W.; Andres, J. L.; Head-Gordon, M.; Replogle, E. S.; Pople, J. A. Gaussian 98, revision A.7; Gaussian, Inc.: Pittsburgh, PA, 1998.

(68) Morris, G. M.; Goodsell, D. S.; Halliday, R. S.; Huey, R.; Hart, W. E.; Belew, R. K.; Olson, A. J. Automated docking using a Lamarckian genetic algorithm and and empirical binding free energy function. *J. Comput. Chem.* **1998**, *19*, 1639–1662.

(69) Sanner, M. F. Python: a programming language for software integration and development. *J. Mol. Graphics Modell.* **1999**, *17*, 57–61.

(70) Huey, R.; Morris, G. M.; Olson, A. J.; Goodsell, D. S. A semiempirical free energy force field with charge-based desolvation. *J. Comput. Chem.* **2007**, *28*, 1145–1152.